Nucleon form factors of the energy-momentum tensor in the chiral quark-soliton model

K. Goeke,[1] J. Grabis,[1] J. Ossmann,[1] M. V. Polyakov,[1,2] P. Schweitzer,[1] A. Silva,[3,4] and D. Urbano[3,4]

[1]*Institut für Theoretische Physik II, Ruhr-Universität Bochum, 44780 Bochum, Germany*

[2]*Petersburg Nuclear Physics Institute, Gatchina, St. Petersburg 188350, Russia*

[3]*Departamento de Física and Centro de Física Computacional, Universidade de Coimbra, P-3000 Coimbra, Portugal*

[4]*Faculdade de Engenharia da Universidade do Porto, P-4000 Porto, Portugal*

(Received 27 February 2007; published 29 May 2007)

The nucleon form factors of the energy-momentum tensor are studied in the large-N_c limit in the framework of the chiral quark-soliton model.

DOI: 10.1103/PhysRevD.75.094021 PACS numbers: 13.60.Hb, 11.15.Pg, 12.38.Lg, 12.39.Fe

I. INTRODUCTION

The nucleon form factors of the energy-momentum tensor (EMT) [1] were subject to modest interest in literature for a long time—probably because the only known process, where they (in principle) could directly be ''measured'' is elastic scattering of gravitons off the nucleon. The situation changed, however, with the advent of generalized parton distribution functions (GPDs) [2–5] accessible in hard exclusive reactions [6–14], see [15–20] for reviews. The form factors of the quark part of the EMT of QCD—we use the notation $M_2^Q(t)$, $J^Q(t)$, and $d_1^Q(t)$, see the definition below in Eq. (1)—appear as certain Mellin moments of the unpolarized quark GPDs.

The form factor $M_2^Q(0)$ is known at zero-momentum transfer from inclusive deeply inelastic scattering experiments, telling us that quarks carry only about half of the momentum of (a very fast moving) nucleon, and that the rest is carried by gluons. The appealing perspective is to access by means of GPDs information on $J^Q(t)$, which—after extrapolating to zero-momentum transfer $t = 0$—would reveal how much of the nucleon spin is due to quarks [3]. The third form factor, $d_1(t)$, is equally interesting—promising to provide information on the distribution of strong forces in the nucleon [21,22] similarly as the electromagnetic form factors contain information about the electric charge distribution [23]. The information content encoded in GPDs is, however, larger than that; see Refs. [24–26].

In this work we study the form factors of the EMT in the framework of the chiral quark-soliton model (CQSM) [27,28]. The model provides a field theoretic description of the nucleon in the limit of a large number of colors N_c, where the nucleon appears as a chiral soliton of a static background pion field [29]. Numerous nucleonic properties, among others, form factors [30–33], usual quark, and antiquark distribution functions [34–39] and GPDs [40–46] have been described in this model without adjustable parameters. As far as those quantities are known an agreement with phenomenology was observed typically to within an accuracy of (10–30)%.

Our study provides several new results. In particular, we compute the spatial density distributions and mean square radii of the operators of different components of the energy-momentum tensor and its trace. This provides insights not only on, for example, how the ''mass'' or the ''angular momentum'' are distributed in the nucleon. Of particular interest are the results for the spatial distribution of strong forces in the nucleon. As a by-product we learn how the soliton acquires stability in the CQSM. We also observe a physically appealing connection between the criterion for the stability of the nucleon and the sign of the form factor $d_1(t)$ at zero-momentum transfer.

We present results for the form factors which are of practical interest especially in the case of $J^Q(t)$. As exclusive reactions yield information on $J^Q(t)$ only at finite $t < 0$, some guidance from reliable model calculation might be of interest for the extrapolation $t \to 0$ required to conclude how much quarks contribute to the nucleon spin.

We explore the chiral character of the model to study chiral properties of the form factors. In particular, we derive the leading nonanalytic chiral contributions to the form factors in the large N_c limit. These nonanalytic (in the current quark mass) terms are model-independent. In fact, our results coincide with results from chiral perturbation theory [47–49], provided one takes into account that the latter is formulated for finite $N_c = 3$ [50,51].

The implicit pion mass dependence of the form factors is of interest in the context of the chiral extrapolation of lattice QCD data [52–57]. This topic can be addressed in the CQSM [58] which will be done in a separate work [59].

For completeness we remark that the general chiral structure of the pion EMT was discussed in chiral perturbation theory and/or chiral models in [60–62]. Issues of pion EMT form factors in lattice QCD were addressed in [63,64].

The paper is organized as follows. Section II provides a general discussion of the EMT form factors. Section III introduces the model. In Sec. IV we derive the model expressions for the form factors and discuss the numerical results for the densities of the static EMT in Secs. V, VI, and VII. In Sec. VIII we present the results for the form factors and conclude our findings in Sec. IX. The appendices contain a digression on alternative notations, a dis-

cussion of general properties of the densities of the static EMT, technical details on the model expressions, and explicit proofs for the consistency of the model.

II. FORM FACTORS OF THE ENERGY-MOMENTUM TENSOR

The nucleon matrix element of the symmetric energy-momentum tensor of QCD is characterized by three scalar form factors [1,3]. The nucleon matrix elements of the quark and gluon parts of the symmetric QCD energy-momentum tensor can be parameterized as [3,21] (see Appendix A for an alternative notation)

$$\begin{aligned}\langle p'|\hat{T}^{Q,G}_{\mu\nu}(0)|p\rangle = \bar{u}(p')\Big[& M_2^{Q,G}(t)\frac{P_\mu P_\nu}{M_N} \\ & + J^{Q,G}(t)\frac{i(P_\mu\sigma_{\nu\rho}+P_\nu\sigma_{\mu\rho})\Delta^\rho}{2M_N} \\ & + d_1^{Q,G}(t)\frac{\Delta_\mu\Delta_\nu - g_{\mu\nu}\Delta^2}{5M_N} \pm \bar{c}(t)g_{\mu\nu}\Big]u(p).\end{aligned} \tag{1}$$

Here $\hat{T}^Q_{\mu\nu}$ ($\hat{T}^G_{\mu\nu}$) is the quark (gluon) part of the QCD energy-momentum tensor. The nucleon states and spinors are normalized by $\langle p'|p\rangle = 2p^0(2\pi)^3\delta^{(3)}(\mathbf{p}'-\mathbf{p})$ and $\bar{u}(p)u(p) = 2M_N$ where we suppress spin indices for brevity. The kinematical variables are defined as $P = (p+p')/2$, $\Delta = (p'-p)$, $t = \Delta^2$. The form factor $\bar{c}(t)$ accounts for nonconservation of the separate quark and gluon parts of the EMT and enters the quark and gluon parts with opposite signs such that the total (quark + gluon) EMT is conserved.

The nucleon form factors of the EMT are related to the unpolarized GPDs $H^f(x,\xi,t)$ and $E^f(x,\xi,t)$, which are defined as

$$\begin{aligned}\int\frac{d\lambda}{2\pi}e^{i\lambda x}\left\langle \mathbf{p}',s'\left|\bar{\psi}_q\left(-\frac{\lambda n}{2}\right)\not{n}\left[-\frac{\lambda n}{2},\frac{\lambda n}{2}\right]\psi_q\left(\frac{\lambda n}{2}\right)\right|\mathbf{p},s\right\rangle \\ = H^q(x,\xi,t)\bar{u}(\mathbf{p}',s')\not{n}u(\mathbf{p},s) \\ + E^q(x,\xi,t)\bar{u}(\mathbf{p}',s')\frac{i\sigma^{\mu\nu}n_\mu\Delta_\nu}{2M_N}u(\mathbf{p},s),\end{aligned} \tag{2}$$

where $[z_1,z_2]$ denotes the gauge link, and the renormalization scale dependence is not indicated for brevity. The lightlike vector n^μ satisfies $n(p'+p)=2$, and the skewedness parameter ξ is defined as $n\Delta = -2\xi$. To be specific, the form factors in Eq. (1) are related to the second Mellin moments of the unpolarized GPDs in (2) through [3]

$$\int_{-1}^{1}dx x\sum_f H^f(x,\xi,t) = M_2^Q(t) + \frac{4}{5}d_1^Q(t)\xi^2, \tag{3}$$

$$\int_{-1}^{1}dx x\sum_f E^f(x,\xi,t) = 2J^Q(t) - M_2^Q(t) - \frac{4}{5}d_1^Q(t)\xi^2. \tag{4}$$

Adding up Eqs. (3) and (4) one recovers the spin sum rule [3] promising to access $J^Q(0)$, i.e. the total (spin + orbital angular momentum) contribution of quarks to the nucleon spin, through the extraction of GPDs from hard exclusive processes and extrapolation to the unphysical point $t=0$. The sensitivity of different observables to the total angular momentum of, in particular, the u flavor, were exposed in the model studies [17,65]. For gluons there are definitions and expressions analog to (2)–(4). Equations (3) and (4) are special cases of the so-called polynomiality property of GPDs [15] stating that the Nth Mellin moments of GPDs are polynomials in even powers of ξ of degree less or equal to N:

$$\begin{aligned}\int_{-1}^{1}\mathrm{d}x x^{N-1}H(x,\xi,t) = h_0^{(N)}(t) + h_2^{(N)}(t)\xi^2 + \ldots \\ + \begin{cases} h_N^{(N)}(t)\xi^N & \text{for } N \text{ even} \\ h_{N-1}^{(N)}(t)\xi^{N-1} & \text{for } N \text{ odd,}\end{cases}\end{aligned} \tag{5}$$

$$\begin{aligned}\int_{-1}^{1}\mathrm{d}x x^{N-1}E(x,\xi,t) = e_0^{(N)}(t) + e_2^{(N)}(t)\xi^2 + \ldots \\ + \begin{cases} e_N^{(N)}(t)\xi^N & \text{for } N \text{ even} \\ e_{N-1}^{(N)}(t)\xi^{N-1} & \text{for } N \text{ odd,}\end{cases}\end{aligned} \tag{6}$$

where flavor indices are suppressed for brevity. For a spin $\frac{1}{2}$ particle, the coefficients in front of the highest power in ξ for even moments N are related to each other and arise from the so-called D term $D^q(z,t)$ with $z = x/\xi$ [66,67], which has finite support only for $|x| < |\xi|$, according to

$$h_N^{q(N)}(t) = -e_N^{q(N)}(t) = \int_{-1}^{1}\mathrm{d}z z^{N-1}D^q(z,t). \tag{7}$$

The form factors of the EMT in Eq. (1) can be interpreted [21] in analogy to the electromagnetic form factors [23] in the Breit frame characterized by $\Delta^0 = 0$. In this frame one can define the static energy-momentum tensor for quarks (and analogously for gluons)

$$T^Q_{\mu\nu}(\mathbf{r},\mathbf{s}) = \frac{1}{2E}\int\frac{\mathrm{d}^3\boldsymbol{\Delta}}{(2\pi)^3}\exp(i\boldsymbol{\Delta}\mathbf{r})\langle p',S'|\hat{T}^Q_{\mu\nu}(0)|p,S\rangle, \tag{8}$$

with the initial and final polarization vectors of the nucleon S and S' defined such that they are equal to $(0,\mathbf{s})$ in the respective rest frame, where the unit vector $\mathbf{s}$ denotes the quantization axis for the nucleon spin.

The components of $T^Q_{0k}(\mathbf{r},\mathbf{s})$ and $\varepsilon^{ijk}r_jT^Q_{0k}(\mathbf{r},\mathbf{s})$ correspond, respectively, to the distribution of quark momentum and quark angular momentum inside the nucleon. The

components of $(T^Q_{ik} - \frac{1}{3}\delta_{ik}T^Q_{ll})(\mathbf{r},\mathbf{s})$ characterize the spatial distribution of "shear forces" experienced by quarks inside the nucleon. The respective form factors are related to $T^Q_{\mu\nu}(\mathbf{r},\mathbf{s})$ by

$$J^Q(t) + \frac{2t}{3}J^{Q'}(t) = \int \mathrm{d}^3\mathbf{r} e^{-i\mathbf{r}\boldsymbol{\Delta}}\varepsilon^{ijk}s_i r_j T^Q_{0k}(\mathbf{r},\mathbf{s}), \tag{9}$$

$$d_1^Q(t) + \frac{4t}{3}d_1^{Q'}(t) + \frac{4t^2}{15}d_1^{Q''}(t) = -\frac{M_N}{2}\int \mathrm{d}^3\mathbf{r} e^{-i\mathbf{r}\boldsymbol{\Delta}}T^Q_{ij}(\mathbf{r})\left(r^i r^j - \frac{\mathbf{r}^2}{3}\delta^{ij}\right), \tag{10}$$

$$M_2(t) - \frac{t}{4M_N^2}\left(M_2(t) - 2J(t) + \frac{4}{5}d_1(t)\right) = \frac{1}{M_N}\int \mathrm{d}^3\mathbf{r} e^{-i\mathbf{r}\boldsymbol{\Delta}}T_{00}(\mathbf{r},\mathbf{s}), \tag{11}$$

where the prime denotes derivative with respect to the Mandelstam variable t. Note that for a spin-1/2 particle only the $T^{0\mu}$ components are sensitive to the polarization vector. Note also that Eq. (11) holds for the sum $T_{00} \equiv T^Q_{00} + T^G_{00}$ with $M_2(t) \equiv M_2^Q(t) + M_2^G(t)$ and $J(t)$ and $d_1(t)$ defined analogously, but not for the separate quark and gluon contributions—since otherwise the form factor $\bar{c}(t)$ would not cancel out.

The form factor $M_2(t)$ at $t = 0$ can be connected to the fractions of the nucleon momentum carried, respectively, by quarks and gluons. This can be seen most conveniently by considering (1) in the infinite momentum frame, and one obtains

$$M_2^Q(0) = \int_0^1 \mathrm{d}x \sum_q x(f_1^q + f_1^{\bar{q}})(x), \qquad M_2^G(0) = \int_0^1 \mathrm{d}x x f_1^g(x), \tag{12}$$

where $f_1^a(x) = H^a(x,0,0)$ are the unpolarized parton distributions accessible in inclusive deeply inelastic scattering.

The form factors $M_2^{Q,G}(t)$, $J^{Q,G}(t)$, and $d_1^{Q,G}(t)$ are renormalization scale dependent (the indication of the renormalization scale μ is suppressed for brevity). Their quark + gluon sums, however, are scale independent form factors, which at $t = 0$ satisfy the constraints,

$$M_2(0) = \frac{1}{M_N}\int \mathrm{d}^3\mathbf{r} T_{00}(\mathbf{r},\mathbf{s}) = 1, \qquad J(0) = \int \mathrm{d}^3\mathbf{r}\varepsilon^{ijk}s_i r_j T_{0k}(\mathbf{r},\mathbf{s}) = \frac{1}{2}, \qquad d_1(0) = -\frac{M_N}{2}\int \mathrm{d}^3\mathbf{r} T_{ij}(\mathbf{r})\left(r^i r^j - \frac{\mathbf{r}^2}{3}\delta^{ij}\right) \equiv d_1, \tag{13}$$

which mean that in the rest frame the total energy of the nucleon is equal to its mass, and that the spin of the nucleon is 1/2. The value of d_1 is not known *a priori* and must be determined experimentally. However, being a conserved quantity it is to be considered on the same footing as other basic nucleon properties like mass, anomalous magnetic moment, etc. Remarkably, d_1 determines the behavior of the D term (and thus the unpolarized GPDs) in the asymptotic limit of renormalization scale $\mu \to \infty$ [17].

The form factor $d_1(t)$ is connected to the distribution of pressure and shear forces experienced by the partons in the nucleon [21] which becomes apparent by recalling that $T_{ij}(\mathbf{r})$ is the static stress tensor which (for spin 0 and 1/2 particles) can be decomposed as

$$T_{ij}(\mathbf{r}) = s(r)\left(\frac{r_i r_j}{r^2} - \frac{1}{3}\delta_{ij}\right) + p(r)\delta_{ij}. \tag{14}$$

The functions $p(r)$ and $s(r)$ are related to each other due to the conservation of the total energy-momentum tensor by the differential equation

$$\frac{2}{3}\frac{\partial s(r)}{\partial r} + \frac{2s(r)}{r} + \frac{\partial p(r)}{\partial r} = 0. \tag{15}$$

Hereby $p(r)$ describes the radial distribution of the "pressure" inside the hadron, while $s(r)$ is related to the distribution of the "shear forces" [21]. Another important property which can be directly derived from the conservation of the EMT is the so-called stability condition. Integrating $\int \mathrm{d}^3\mathbf{r} r^k(\nabla_i T^{ij}) \equiv 0$ by parts one finds that the pressure $p(r)$ must satisfy the relation

$$\int_0^\infty \mathrm{d}r r^2 p(r) = 0. \tag{16}$$

Further, it is worthwhile noticing properties which follow from the conservation of the EMT; these are discussed in Appendix B. Here we only mention that one can express $d_1(t)$ in terms of $p(r)$ and $s(r)$ as (notice the misprint in Eq. (18) of [22])

$$d_1(t) = 5M_N\int \mathrm{d}^3\mathbf{r}\frac{j_2(r\sqrt{-t})}{t}s(r) = 15M_N\int \mathrm{d}^3\mathbf{r}\frac{j_0(r\sqrt{-t})}{2t}p(r), \qquad d_1 = -\frac{1}{3}M_N\int \mathrm{d}^3\mathbf{r} r^2 s(r) = \frac{5}{4}M_N\int \mathrm{d}^3\mathbf{r} r^2 p(r). \tag{17}$$

Let us review briefly what is known about d_1. For the pion $d_{1,\pi}$ can be calculated exactly using soft pion theorems, and one obtains $\frac{4}{5}d^Q_{1,\pi} = -M^Q_{2,\pi}$ [66]. For the nucleon the large-N_c limit predicts [17]

$$|d_1^u + d_1^d| = \mathcal{O}(N_c^2) \gg |d_1^u - d_1^d| = \mathcal{O}(N_c), \tag{18}$$

which is in agreement with lattice QCD [54–56]. The constant $d_1^Q = d_1^u + d_1^d$ is found negative on the lattice [54–56]. From model calculations in the CQSM it was estimated that $d_1^Q \approx -4.0$ at scales of few GeV^2 [40,68]. In a simple "liquid drop" model d_1 is related to the surface

tension of the ''liquid'' and comes out negative [21]. Such a model is, in particular, applicable to large nuclei. Predictions for the behavior of the cross section of deeply virtual Compton scattering off nuclei made on the basis of this model [21] have been confirmed in realistic models for nuclei [69]. In particular, also the D terms of nuclei were found negative [69]. Interestingly, HERMES data [10,14] favor a negative D term though this observation depends to some extent on the model for the small-x behavior of GPDs [19].

Finally, let us discuss an interesting connection of the constant d_1 and the mean square radius $\langle r_F^2\rangle$ of the trace of the total EMT operator. Because of the trace anomaly [70–73], the latter is given by

$$\hat{T}_\mu{}^\mu \equiv \frac{\beta}{2g} F^{\mu\nu}F_{\mu\nu} + (1+\gamma_m)\sum_a m_a \bar{\psi}_a\psi_a. \tag{19}$$

For notational simplicity let us introduce the scalar form factor $F(t)$

$$\langle p'|\hat{T}_\mu{}^\mu(0)|p\rangle = M_N \bar{u}(p')u(p)F(t), \tag{20}$$

which can be expressed in terms of the form factors in (1) as

$$F(t) = M_2(t) + \frac{t}{4M_N^2}(2J(t) - M_2(t)) - \frac{3t}{5M_N^2}d_1(t). \tag{21}$$

It satisfies $F(0) = 1$ and its derivative at $t = 0$ defines the mean square radius of the EMT trace operator

$$\langle r_F^2\rangle = 6F'(0) = 6\left(M_2'(0) - \frac{3d_1}{5M_N^2}\right). \tag{22}$$

Analogously, one may define the mean square radius $\langle r_E^2\rangle$ of the energy density operator $\hat{T}^{00}$ for which one finds from Eq. (11) the following result:

$$\langle r_E^2\rangle = 6\left(M_2'(0) - \frac{d_1}{5M_N^2}\right). \tag{23}$$

Exploring (23) we see that $\langle r_F^2\rangle$ is related to the mean square radius of the energy density $\langle r_E^2\rangle$ as follows:

$$\langle r_F^2\rangle = \langle r_E^2\rangle - \frac{12d_1}{5M_N^2}. \tag{24}$$

Since d_1 is observed to be negative, one has $\langle r_F^2\rangle > \langle r_E^2\rangle$.

III. THE NUCLEON AS A CHIRAL SOLITON

The effective theory underlying the CQSM was derived from the instanton model of the QCD vacuum [74,75] which assumes that the basic properties of the QCD vacuum are dominated by a strongly interacting medium of instantons and anti-instantons. This medium is diluted with a density proportional to $(\rho_{\rm av}/R_{\rm av})^4$ where $\rho_{\rm av} \approx 0.3$ fm is the average instanton size and $R_{\rm av}$ the average instanton separation. It is found $\rho_{\rm av}/R_{\rm av} \sim \frac{1}{3}$ [74–76]; see [77] for reviews.

Because of interactions with instantons in this medium, light quarks acquire a dynamical (''constituent'') quark mass which is strictly speaking momentum dependent, i.e. $M = M(p)$, and drops to zero for momenta $p \gg \rho_{\rm av}^{-1}$. At low momenta below a scale set by $\rho_{\rm av}^{-1} \approx 600$ MeV, the dynamics of these effective quark degrees of freedom is governed by the partition function [78,79]

$$\begin{aligned} Z_{\rm eff} &= \int \mathcal{D}\psi\mathcal{D}\bar{\psi}\mathcal{D}U \exp(iS_{\rm eff}(\bar{\psi},\psi,U)), \\ S_{\rm eff}(\bar{\psi},\psi,U) &= \int {\rm d}^4x \bar{\psi}(i\partial\!\!\!/ - MU^{\gamma_5} - m)\psi. \end{aligned} \tag{25}$$

Here we restrict ourselves to two light flavors, $U = \exp(i\tau^a\pi^a)$ denotes the chiral pion field with $U^{\gamma_5} = \exp(i\gamma_5\tau^a\pi^a)$, and $m = m_u = m_d$ is the current quark mass neglecting isospin breaking effects. The smallness of the instanton packing fraction $\rho_{\rm av}/R_{\rm av}$ plays an important role in the derivation of (25) from the instanton vacuum model.

In practical calculations it is convenient to replace $M(p)$ by a constant mass $M = M(0) = 350$ MeV following from the instanton vacuum [77] and to regularize the effective theory by means of an explicit (e.g. proper-time, or Pauli-Villars) regularization with a cutoff of $\mathcal{O}(\rho_{\rm av}^{-1})$ whose precise value is fixed to reproduce the physical value of the pion decay constant $f_\pi = 93$ MeV given by a logarithmically UV-divergent expression in the effective theory (25). For most quantities the effects of different regularizations are of $\mathcal{O}(M^2\rho_{\rm av}^2) \propto \rho_{\rm av}^4/R_{\rm av}^4$, i.e. parametrically small.

The CQSM is an application of the effective theory (25) to the description of baryons [27,28]. The Gaussian integral over fermion fields in (25) can be solved exactly. The path integral over pion field configurations, however, can be solved only by means of the saddle-point approximation (in the Euclidean formulation of the theory). This step is strictly justified in the large-N_c limit. In the leading order of the large-N_c limit the pion field is static, and one can determine the spectrum of the one-particle Hamiltonian of the effective theory (25)

$$\hat{H}|n\rangle = E_n|n\rangle, \qquad \hat{H} = -i\gamma^0\gamma^k\partial_k + \gamma^0 MU^{\gamma_5} + \gamma^0 m. \tag{26}$$

The spectrum consists of an upper and a lower Dirac continuum, distorted by the pion field as compared to continua of the free Dirac-Hamiltonian $\hat{H}_0$ [which follows from $\hat{H}$ in (26) by replacing $U^{\gamma_5} \to 1$] and of a discrete bound state level of energy $E_{\rm lev}$, if the pion field is strong enough. By occupying the discrete level and the states of the lower continuum each by N_c quarks in an antisymmetric color state, one obtains a state with unity baryon number. The soliton energy $E_{\rm sol}$ is a functional of the pion field

$$E_{\rm sol}[U] = N_c\Big[E_{\rm lev} + \sum_{E_n<0}(E_n - E_{n_0})\Big]_{\rm reg}. \qquad (27)$$

$E_{\rm sol}[U]$ is logarithmically divergent, see Appendix D for the explicit expression in the proper-time regularization. By minimizing $E_{\rm sol}[U]$ one obtains the self-consistent solitonic pion field U_c. This procedure is performed for symmetry reasons in the so-called hedgehog ansatz

$$\pi^a(\mathbf{x}) = e_r^a P(r), \qquad U(\mathbf{x}) = \cos P(r) + i\tau^a e_r^a \sin P(r), \qquad (28)$$

with the radial (soliton profile) function $P(r)$ and $r = |\mathbf{x}|$, $\mathbf{e}_r = \mathbf{x}/r$. The nucleon mass M_N is given by $E_{\rm sol}[U_c]$. The self-consistent profile satisfies $P_c(0) = -\pi$ and behaves as

$$P(r) = -\frac{A}{r^2}(1 + m_\pi r)\exp(-m_\pi r) \quad \text{at large } r,$$
$$\text{with} \quad A = \frac{3g_A}{8\pi f_\pi^2}, \qquad (29)$$

where $g_A = 1.26$ is the axial coupling constant and the pion mass m_π is connected to m in (25) by the Gell-Mann-Oakes-Renner relation for small m. In the large-N_c limit the path integral over U in Eq. (25) is solved by evaluating the expression at U_c and integrating over translational and rotational zero modes of the soliton solution in the path integral. In order to include corrections in the $1/N_c$ expansion, one considers time dependent pion field fluctuations around the solitonic solution. In practice, hereby one restricts oneself to time dependent rotations of the soliton field in spin- and flavor-space which are slow due to the large moment of inertia of the soliton, $I = \mathcal{O}(N_c)$, given by

$$I = \frac{N_c}{6}\sum_{\substack{m,\rm non\\ n,\rm occ}}\frac{\langle n|\tau^a|m\rangle\langle m|\tau^a|n\rangle}{E_m - E_n}\Bigg|_{\rm reg}. \qquad (30)$$

As indicated, I is logarithmically divergent and has to be regularized. In (30) the sum goes over occupied (''occ'') states n which satisfy $E_n \le E_{\rm lev}$, and over nonoccupied (''non'') states m which satisfy $E_m > E_{\rm lev}$.

IV. FORM FACTORS OF THE ENERGY-MOMENTUM TENSOR IN THE CQSM

The gluon part of the EMT is zero in the effective theory (25), since there are no explicit gluon degrees of freedom. Consequently in the model the quark energy-momentum tensor is conserved by itself, and the form factor $\bar{c}(t)$ in Eq. (1) vanishes. This is demonstrated explicitly in Appendix C. The nucleon matrix elements of the effective operator for the quark energy-momentum tensor (we omit in the following the index Q) is given by the path integral

$$\langle p'|\hat{T}_{\mu\nu}(0)|p\rangle = \lim_{T\to\infty}\frac{1}{Z_{\rm eff}}\int {\rm d}^3\mathbf{x}{\rm d}^3\mathbf{y}e^{i\mathbf{p}'\mathbf{y}-i\mathbf{p}\mathbf{x}} \times\int \mathcal{D}\psi\mathcal{D}\bar{\psi}\mathcal{D}U J_{N'}(-T/2,\mathbf{y})\hat{T}^{\rm eff}_{\mu\nu}(0) \times J_N^\dagger(T/2,\mathbf{x})\exp(iS_{\rm eff}(\bar{\psi},\psi,U)), \qquad (31)$$

where $J_N(x)$ denotes the nucleon current; see [28,30,31] for explicit expressions. The symmetric energy-momentum tensor for quarks in the effective theory (25) is given by (the arrows indicate on which fields the derivatives act)

$$\hat{T}^{\rm eff}_{\mu\nu}(x) = \tfrac{1}{4}\bar{\psi}(x)(i\gamma^\mu\vec{\partial}^\nu + i\gamma^\nu\vec{\partial}^\mu - i\gamma^\mu\overleftarrow{\partial}^\nu - i\gamma^\nu\overleftarrow{\partial}^\mu)\psi(x). \qquad (32)$$

For the calculation of the EMT nucleon matrix elements in the model we have to evaluate consistently the nucleon-bispinor expressions appearing on the right-hand side of Eq. (1) in the large-N_c limit where $p^0 = M_N = \mathcal{O}(N_c)$ and $|p^i| = \mathcal{O}(N_c^0)$ such that $|t| \ll M_N^2$. Keeping in mind that in the large-N_c limit the form factors behave as [17]

$$M_2(t) = \mathcal{O}(N_c^0), \qquad J(t) = \mathcal{O}(N_c^0), \qquad d_1(t) = \mathcal{O}(N_c^2), \qquad (33)$$

we obtain from (1) the following relations for the form factors:

$$\langle p', S_3'|T^{00}_{\rm eff}|p, S_3\rangle = 2M_N^2\delta_{S_3'S_3}\Big(M_2(t) - \frac{t}{5M_N^2}d_1(t)\Big), \qquad (34)$$

$$\langle p', S_3'|T^{ik}_{\rm eff}|p, S_3\rangle = 2\delta_{S_3'S_3}(\Delta^i\Delta^k - \delta^{ik}\mathbf{\Delta}^2)d_1(t), \qquad (35)$$

$$\langle p', S_3'|T^{0k}_{\rm eff}|p, S_3\rangle = -iM_N\varepsilon^{klm}\Delta^l\sigma^m_{S_3'S_3}J(t). \qquad (36)$$

The expressions for $M_2(t)$ and $d_1(t)$ could, of course, be separated which we shall do more conveniently at a later stage. Evaluating the respective components of the EMT in (31) yields [vacuum subtraction analog to (27) is implied]

$$\langle p', S_3'|\hat{T}^{00}_{\rm eff}|p, S_3\rangle = \delta_{S_3'S_3}2M_NN_c\sum_{n,\rm occ}E_n\langle n|e^{i\mathbf{\Delta}\hat{\mathbf{x}}}|n\rangle|_{\rm reg}, \qquad (37)$$

$$\langle p', S_3'|\hat{T}^{ik}_{\rm eff}|p, S_3\rangle = \delta_{S_3'S_3}2M_NN_c\sum_{n,\rm occ}\frac{1}{4}\langle n|(\{e^{i\mathbf{\Delta}\hat{\mathbf{x}}}, \gamma^0\gamma^i\hat{p}^k\} + (i\leftrightarrow k))|n\rangle|_{\rm reg}, \qquad (38)$$

$$\langle p', S_3'|\hat{T}^{0k}_{\rm eff}|p, S_3\rangle = \sigma^l_{S_3'S_3}\frac{M_NN_c}{4I}\sum_{\substack{m,\rm occ\\ j,\rm non}}\frac{\langle m|\tau^l|j\rangle}{E_m - E_j} \times\langle j|(\{e^{i\mathbf{\Delta}\hat{\mathbf{x}}}, \hat{p}^k\} + (E_m + E_j)\gamma^0\gamma^k e^{i\mathbf{\Delta}\hat{\mathbf{x}}})|m\rangle|_{\rm reg}. \qquad (39)$$

These expressions are logarithmically divergent and have to be regularized appropriately; see Appendix D for details.

Noteworthy, the matrix elements for the components $\hat{T}^{00}_{\rm eff}$ and $\hat{T}^{0k}_{\rm eff}$ related to $M_2(t)$ and $d_1(t)$ are spin independent and receive contributions from leading order of the large-N_c expansion. In contrast to this, in order to address $\hat{T}^{0k}_{\rm eff}$ connected to $J(t)$ one needs matrix elements involving nucleon spin flip which appear only when considering $1/N_c$ (''rotational'') corrections. Inserting the results (37)–(39) into Eqs. (34)–(36) yields

$$M_2(t) - \frac{t}{5M_N^2} d_1(t) = \frac{N_c}{M_N} \sum_{n,\rm occ} E_n \langle n|e^{i\mathbf{\Delta}\hat{\mathbf{x}}}|n\rangle|_{\rm reg}, \tag{40}$$

$$d_1(t) = \frac{5M_N N_c}{4t} \sum_{n,\rm occ} \langle n|\{\gamma^0\boldsymbol{\gamma}\hat{\mathbf{p}}, e^{i\mathbf{\Delta}\hat{\mathbf{x}}}\}|n\rangle|_{\rm reg}, \tag{41}$$

$$J(t) = \frac{iN_c\varepsilon^{klm}\Delta^k}{8It} \sum_{\substack{n,\rm occ\\ j,\rm non}} \frac{\langle n|\tau^l|j\rangle}{E_j - E_n} \langle j|(\{e^{i\mathbf{\Delta}\hat{\mathbf{x}}}, \hat{p}^m\} + (E_n + E_j)e^{i\mathbf{\Delta}\hat{\mathbf{x}}}\gamma^0\gamma^m)|n\rangle|_{\rm reg}. \tag{42}$$

The derivation of Eqs. (40)–(42) follows closely the derivation of the model expressions for electromagnetic [30] or other form factors, and we omit the details here. Instead, we demonstrate explicitly in Appendices E, F, G, and H that one obtains the same expressions for the form factors from the model expressions for GPDs via the sum rules (3) and (4).

We introduce the Fourier transforms of the form factors which are radial functions (''densities'') defined as

$$\rho_E(r) = N_c \sum_{n,\rm occ} E_n \phi_n^*(\mathbf{r})\phi_n(\mathbf{r})|_{\rm reg}, \tag{43}$$

$$p(r) = \frac{N_c}{3} \sum_{n,\rm occ} \phi_n^*(\mathbf{r})(\gamma^0\boldsymbol{\gamma}\hat{\mathbf{p}})\phi_n(\mathbf{r})|_{\rm reg}, \tag{44}$$

$$\rho_J(r) = -\frac{N_c}{24I} \sum_{\substack{n,\rm occ\\ j,\rm non}} \epsilon^{abc} r^a \phi_j^*(\mathbf{r})(2\hat{p}^b + (E_n + E_j)\gamma^0\gamma^b)\phi_n(\mathbf{r}) \frac{\langle n|\tau^c|j\rangle}{E_j - E_n}\Big|_{\rm reg}, \tag{45}$$

where it is understood that $\hat{p}^j \equiv \frac{i}{2}(\overleftarrow{\nabla}^j - \vec{\nabla}^j)$, and which allow us to reexpress $M_2(t)$, $J(t)$, and $d_1(t)$ in (40)–(42) as

$$M_2(t) - \frac{t}{5M_N^2} d_1(t) = \frac{1}{M_N} \int {\rm d}^3\mathbf{r}\rho_E(r) j_0(r\sqrt{-t}), \tag{46}$$

$$d_1(t) = \frac{15M_N}{2} \int {\rm d}^3\mathbf{r} p(r) \frac{j_0(r\sqrt{-t})}{t}, \tag{47}$$

$$J(t) = 3 \int {\rm d}^3\mathbf{r}\rho_J(r) \frac{j_1(r\sqrt{-t})}{r\sqrt{-t}}. \tag{48}$$

Here $j_k(z)$ denote Bessel functions with $j_0(z) = \frac{\sin z}{z}$ and $j_1(z) = -j_0'(z)$.

The densities (43)–(45) are convenient not only because their numerical evaluation is more economic than the direct calculation of the form factors (40)–(42). These densities are interesting objects by themselves, and it is instructive to discuss their theoretical properties in detail which we shall do in the following. Simultaneously we will present the numerical results for the densities.

For the numerical calculation we employ the so-called Kahana-Ripka method [80], whose application to calculations in the CQSM is described in detail e.g. in Ref. [31], and use the proper-time regularization. The latter allows us to include effects of symmetry breaking due to an explicit chiral symmetry breaking current quark mass m in the effective action (25) and to study in the model how observables vary in the chiral limit. (For a study—in the spirit of [58]—of observables at pion masses as large as they appear in present day lattice calculations, the reader is referred to [59].)

TABLE I. The pion mass dependence of different quantities computed in the CQSM: the energy density in the center of the nucleon $\rho_E(0)$; the mean square radii $\langle r_E^2\rangle$ and $\langle r_J^2\rangle$ as defined in Eqs. (51) and (56); the pressure $p(0)$ in the center of the nucleon; the zero of the pressure defined as $p(r_0) = 0$; the constant d_1; the dipole masses of the form factors $M_2(t)$, $J(t)$, and $d_1(t)$ as defined in Eq. (71); and the mean squared radius of the trace of the EMT (22). In the chiral limit $J(t)$ and $d_1(t)$ have infinitely steep slopes at $t = 0$. In these cases dipole fits do not provide useful approximations and are undefined (labeled by ''—'' in the table). The proper-time regularization can be applied, in principle, to any m_π [58]. The Pauli-Villars regularization is applicable only for $m_\pi = 0$ [81].

m_π	$\rho_E(0)$	$\langle r_E^2\rangle$	$\langle r_J^2\rangle$	$p(0)$	r_0	d_1	Dipole masses $M_{\rm dip}$ in GeV for			$\langle r_F^2\rangle$
MeV	GeV/fm^3	fm^2	fm^2	GeV/fm^3	fm		$M_2(t)$	$J(t)$	$d_1(t)$	fm^2
Proper-time regularization:										
0	1.54	0.79	∞	0.195	0.59	−3.46	0.867	—	—	1.01
50	1.57	0.76	1.42	0.202	0.59	−3.01	0.873	0.692	0.519	0.95
140	1.70	0.67	1.32	0.232	0.57	−2.35	0.906	0.745	0.646	0.81
Pauli-Villars regularization:										
0	0.75	0.86	∞	0.332	0.63	−4.75	0.804	—	—	1.24

In order to explore effects of different regularizations, we perform also a calculation with the Pauli-Villars regularization method which, however, is applicable only in the chiral limit [81]. All results are summarized in Table I.

V. ENERGY DENSITY

The density $\rho_E(r)$ is just the energy density $T^{00}(r)$ in the static energy-momentum tensor (8). By using the orthonormality of the single-quark states $\int d^3\mathbf{r}\phi_n^*(\mathbf{r})\phi_{n'}(\mathbf{r}) = \delta_{nn'}$ and comparing to Eq. (27) we find that

$$\int d^3\mathbf{r}\rho_E(r) = N_c \sum_{n,\mathrm{occ}} E_n \int d^3\mathbf{r}\phi_n^*(\mathbf{r})\phi_n(\mathbf{r})|_{\mathrm{reg}} = M_N. \tag{49}$$

The normalization (49) ensures the correct constraint of the form factor $M_2(t)$ at $t = 0$. In fact, by taking in Eq. (46) the limit $t \to 0$ [notice that $d_1(t)$ takes a well-defined finite value for $t \to 0$, see below] we obtain

$$M_2(0) = \frac{1}{M_N}\int d^3\mathbf{r}\rho_E(r) = 1. \tag{50}$$

This is the consistent constraint in the model for $M_2(t)$ at $t = 0$, cf. Eq. (12), since there are no gluons in the effective theory such that consequently the entire momentum of the nucleon is carried by quarks and antiquarks [34].

Figure 1(a) shows the normalized density $\rho_E(r)/M_N$ as a function of r for the physical situation with a pion mass of 140 MeV. In this case in the model the nucleon mass is about 1250 MeV. This overestimate of the physical nucleon mass of $\mathcal{O}(300$ MeV) is typical for the soliton approach and its origin is well understood [82]. In the center of the nucleon one finds $\rho_E(0) = 1.7$ GeV fm^{-3} or 3.0×10^{15} g cm^{-3}. In order to gain some intuition about this number we remark that this corresponds roughly to 13 times the equilibrium density of nuclear matter.

It is instructive to consider the energy density in the chiral limit. The result is shown in Fig. 1(b) where we compare $4\pi r^2\rho_E(r)/M_N$ as functions of r for $m_\pi = 0$ and 140 MeV. The curves are normalized such that one obtains unity when integrating over r. Figure 1(b) shows that with decreasing m_π the energy density is spread more widely. This can be quantified by considering the m_π dependence of the mean square radius of the energy density (23) defined as

$$\langle r_E^2\rangle = \frac{\int d^3\mathbf{r}r^2\rho_E(r)}{\int d^3\mathbf{r}\rho_E(r)}, \tag{51}$$

and which increases in the chiral limit, see Table I. This is an intuitively expected feature. As the pion mass decreases, the range of the "pion cloud" increases and the nucleon becomes "larger."

The popular idea of the nucleon consisting of a "quark core" surrounded by a "pion cloud" is strictly speaking well defined in models only. Here, in the CQSM, we shall associate the contribution of the discrete level as "quark core" and the contribution of the negative continuum states as "pion cloud." From the long-distance behavior of the soliton profile (29) one finds in the chiral limit

$$\rho_E(r) = \frac{f_\pi^2}{4}\,\mathrm{tr}_F[\nabla^k U(\mathbf{r})\nabla^k U^\dagger(\mathbf{r})] + \ldots \overset{r\to\text{large}}{\to} 3\left(\frac{3g_A}{8\pi f_\pi}\right)^2\frac{1}{r^6}, \tag{52}$$

where tr_F is the trace over flavor indices of the SU(2) matrices and the dots in the intermediate step denote terms which contain higher U-field derivative terms and vanish faster at large r than the displayed leading term. The result (52) can be read off from Eq. (7.8) of [34]. At $m_\pi \neq 0$ the decay of $\rho_E(r)$ at large r is exponential due to the corresponding behavior of the soliton profile (29). This diminishes the "range of the pion cloud" and reduces $\langle r_E^2\rangle$.

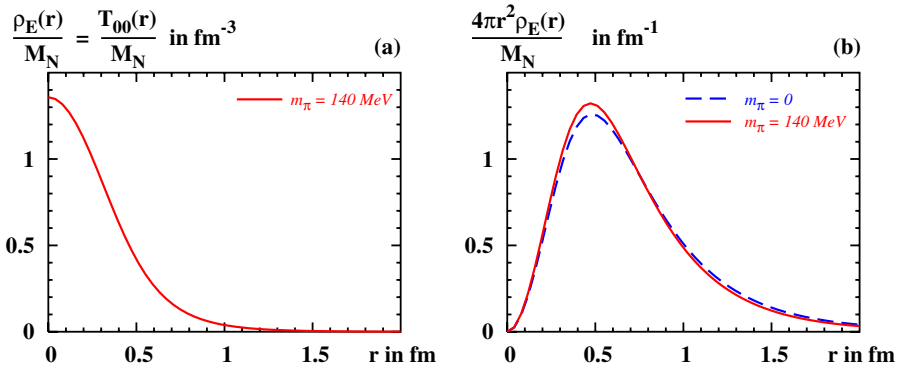

FIG. 1 (color online). (a) The normalized energy density $\rho_E(r)/M_N$ of the nucleon as a function of r for the physical situation with $m_\pi = 140$ MeV. The curve is normalized such that it yields unity upon integration over the entire volume. (b) The normalized energy density $4\pi r^2\rho_E(r)/M_N$ as a function of r in the chiral limit and for $m_\pi = 140$ MeV. The curves are normalized such that one obtains unity upon integration over r.

These observations can be further quantified by considering the chiral expansion of (51) which gives, see Appendix I,

$$\langle r_E^2\rangle = \langle \mathring{r}_E^2\rangle - \frac{81 g_A^2}{64\pi f_\pi^2 M_N} m_\pi + \ldots \tag{53}$$

Here and in the following the $\circ$ above a quantity denotes its value in the chiral limit, and the dots denote terms vanishing faster in the chiral limit than the respective leading term. Considering the noncommutativity of the limits $N_c \to \infty$ and $m_\pi \to 0$ (see the discussion below in Sec. VIII) Eq. (53) agrees with chiral perturbation theory [48].

The term linear in m_π in Eq. (53), i.e. the leading nonanalytic (in the current quark mass $m \propto m_\pi^2$) contribution to the mean square radius of the energy density accounts almost entirely for the reduction of $\langle r_E^2\rangle$ from $m_\pi = 0$ to 140 MeV; see Table I.[1] At the physical pion mass we find $\langle r_E^2\rangle = 0.67$ fm^2. This value is similar to the electric charge radius of the proton. In fact, we observe a qualitative similarity of the energy density and electric proton charge distributions in the model [30,31].

VI. ANGULAR MOMENTUM DENSITY

Taking in Eq. (48) the limit $t \to 0$ yields

$$J(0) = \int \mathrm{d}^3\mathbf{r}\,\rho_J(r), \tag{54}$$

which shows in which sense it is adequate to refer to $\rho_J(r)$ as the ''angular momentum density.'' In order to see that $J(0) = \frac{1}{2}$, i.e. that the constraint (13) is satisfied in the CQSM we insert (45) in the above equation and obtain

$$\begin{aligned} 2J(0) &= \frac{N_c}{12I}\sum_{\substack{n,\mathrm{occ}\\ j,\mathrm{non}}} \epsilon^{abc}\langle j|(2\hat{p}^a\hat{r}^b + (E_n + E_j)\gamma^0\gamma^a\hat{r}^b)|n\rangle \\ &\quad \times \frac{\langle n|\tau^c|j\rangle}{E_j - E_n}\Big|_{\mathrm{reg}} \\ &\overset{\text{Ref. [44]}}{=} \int_{-1}^{1} dx \sum_f (H^f + E^f)(x,\xi,0) \overset{\text{Ref. [44]}}{\equiv} 1. \end{aligned} \tag{55}$$

In the intermediate step in Eq. (55), we recovered the model expression for the second moment of $\sum_f (H^f + E^f)(x,\xi,t)$ at $t = 0$; see Appendix C of [44]. This sum rule, which follows from adding up Eqs. (3) and (4), was explicitly proven to be satisfied in the model in [44]. In the model the entire nucleon spin is due to the spin and orbital angular momentum of quarks and antiquarks, and hence $2J(0) = 1$ [44]. This again is a correct and consistent result since there are no explicit gluon degrees of freedom in the CQSM.

The numerical result for the normalized angular momentum density $\rho_J(r)/J_N \equiv 2\rho_J(r)$ as a function of r for the physical situation is shown in Fig. 2(a). ($J_N = \frac{1}{2}$ denotes the nucleon spin). We observe that $\rho_J(r) \propto r^2$ at small r.

In Fig. 2(b) we compare the normalized angular momentum densities $4\pi r^2\rho_J(r)/J_N$ as functions of r for $m_\pi = 0$ and 140 MeV. These curves are normalized such that one obtains unity upon integration over r. Within the rotating soliton picture the result is reasonable. The smaller m_π, the larger the nucleon, and the more important is the role of the region of large r for the description of the soliton rotation, i.e. for the spin structure of the nucleon. This is reflected by the mean square radius of the angular momentum density which we define in analogy to (51) as

$$\langle r_J^2\rangle = \frac{\int \mathrm{d}^3\mathbf{r} r^2\rho_J(r)}{\int \mathrm{d}^3\mathbf{r}\rho_J(r)}. \tag{56}$$

The mean square radius of the angular momentum density increases with decreasing m_π; see Table I. In the chiral limit $\rho_J(r) \propto \frac{1}{r^4}$ at large r, i.e. $\langle r_J^2\rangle$ diverges in the chiral limit. As a consequence $J(t)$ has an infinitely steep slope at $t = 0$ in the chiral limit; see Sec. VIII and Appendix I for further discussions.

VII. PRESSURE, SHEAR FORCES, SOLITON STABILITY, AND SIGN OF d_1

For the pressure (44) the analogon of the ''normalization relations,'' Eqs. (49) and (55), of the other densities is the stability criterion (16). Integrating the r^2-weighted model expression for $p(r)$ over r we obtain

$$\begin{aligned} \int_0^\infty \mathrm{d}r r^2 p(r) &\equiv \frac{N_c}{12\pi}\int \mathrm{d}^3\mathbf{x}\sum_{n,\mathrm{occ}} \phi_n^*(\mathbf{x})(\gamma^0\boldsymbol{\gamma}\hat{\mathbf{p}})\phi_n(\mathbf{x}) \\ &= \frac{N_c}{12\pi}\sum_{n,\mathrm{occ}}\langle n|\gamma^0\boldsymbol{\gamma}\hat{\mathbf{p}}|n\rangle = 0, \end{aligned} \tag{57}$$

because more generally the tensor K^{ij} defined as

$$K^{ij} = \sum_{n,\mathrm{occ}}\langle n|\gamma^0\gamma^i\hat{p}^j|n\rangle \overset{\text{Ref. [34]}}{=} 0 \tag{58}$$

is zero—however, if and only if, one evaluates the expression (58) with the self-consistent profile, i.e. with that profile which minimizes the soliton energy (27). This was proven in Ref. [34]. Thus, the stability criterion (16) is satisfied.

Next let us check that one obtains in the model the correct result for the constant $d_1 = d_1(0)$ defined in Eq. (13). Expanding the expression (47) around small t we obtain

[1] In the CQSM the physical value of g_A is underestimated by about 30% in the proper-time regularization in the leading order of the $1/N_c$ expansion to which we work here. For consistency we have to use here this leading order N_c model result for g_A. Including $1/N_c$ corrections the model describes g_A more accurately [31].

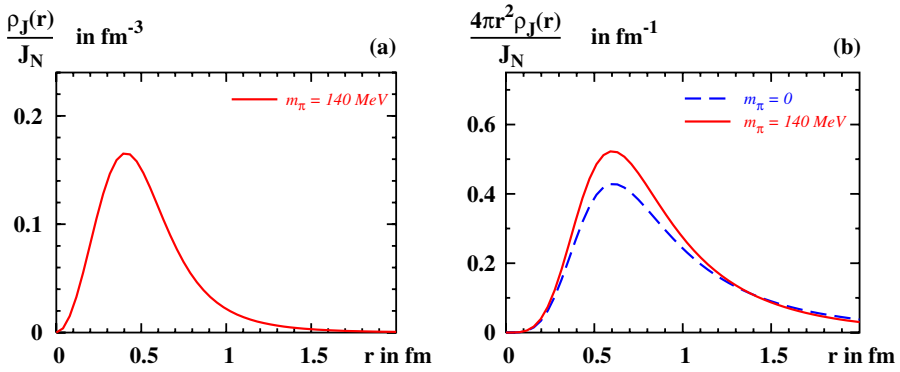

FIG. 2 (color online). (a) The normalized angular momentum density $\rho_J(r)/J_N$ as a function of r for the physical situation with $m_\pi = 140$ MeV. The curve is normalized such that it yields unity upon integration over the entire volume. (b) The normalized angular momentum density $4\pi r^2 \rho_J(r)/J_N$ as a function of r for $m_\pi = 0$ and 140 MeV. The curves are normalized such that one obtains unity upon integration over r.

$$d_1(t) = \frac{15 M_N}{2} \int \mathrm{d}^3\mathbf{r}\, p(r)\left(\frac{1}{t} + \frac{r^2}{3!} + \mathcal{O}(t)\right). \tag{59}$$

Because of (57) the $1/t$ term drops out, and we verify in the CQSM the relation (17) between d_1 and the pressure.

Figure 3(a) shows the pressure $p(r)$ as a function of r. In the physical situation $p(r)$ takes its global maximum at $r = 0$ with $p(0) = 0.23$ GeV/fm^3 $= 3.7 \cdot 10^{34}$ Pa. This is $\mathcal{O}$(10–100) higher than the pressure inside a neutron star [83]. Then $p(r)$ decreases monotonically—becoming zero at $r_0 = 0.57$ fm—till reaching its global minimum at $r_{p,\mathrm{min}} = 0.72$ fm, after which it increases monotonically remaining, however, always negative. The positive sign of the pressure for $r < r_0$ corresponds to repulsion, while the negative sign in the region $r > r_0$ means attraction.

In Fig. 3(a) we see how the pressure depends on the pion mass. The pressure in the center of the nucleon increases as m_π increases—obvious consequence of the fact that the (energy) density also increases, see Table I. As a response to the increased $p(r)$ at small r—keep in mind the stability condition (16)—the pressure takes also larger absolute values in the region $r > r_0$ where it is negative. This can again be intuitively understood because a heavier particle is more tightly bound, i.e. the attractive forces are stronger. The zero of $p(r)$ moves towards smaller values of r with increasing m_π, see Table I.

In Fig. 3(b) we show the distribution of the shear forces $s(r)$ obtained from our results for $p(r)$ by solving the differential Eq. (15). The distribution of shear forces is always positive. It reaches for $m_\pi = 140$ MeV a global maximum at $r = 0.40$ fm. The position of the maximum is weakly dependent on m_π. At small r we observe $s(r) \propto r^2$.

It is interesting to compare to which extent the nucleon "resembles" a liquid drop of radius R_d with constant density and constant pressure p_0 inside. In such a drop the pressure and shear forces are given by [21]

$$p(r) = p_0\theta(R_d - r) - \tfrac{1}{3} p_0 R_d \delta(R_d - r) \quad \text{and} \quad s(r) = \gamma\delta(R_d - r), \tag{60}$$

where $\gamma = \frac{1}{2} p_0 R_d$ denotes the surface tension. We show

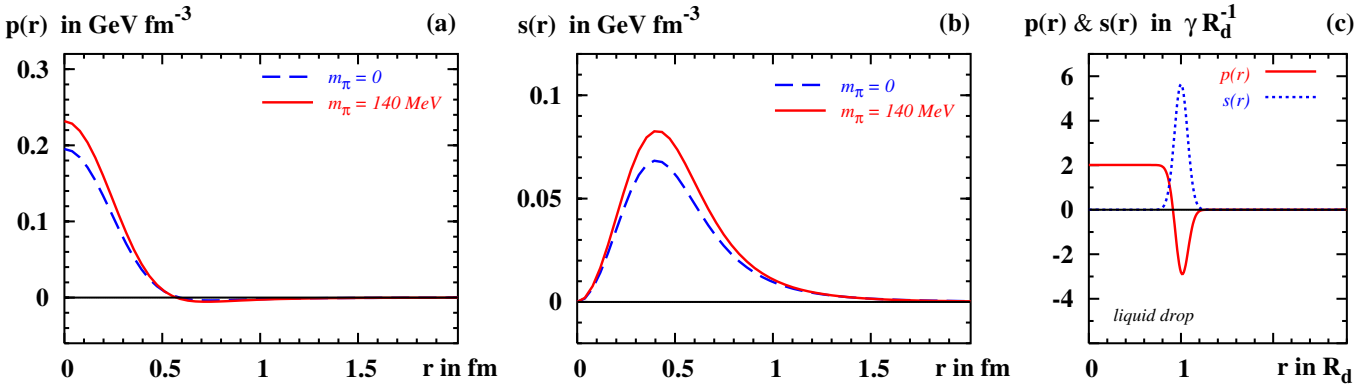

FIG. 3 (color online). (a) The pressure $p(r)$ as a function of r for $m_\pi = 0$ and 140 MeV. (b) The same for the function $s(r)$ defined in Eq. (14) which describes the shear forces in the nucleon and is related to $p(r)$ by the relation (15). (c) $p(r)$ and $s(r)$ in a liquid drop in units of γ/R_d as functions of r in units of R_d. Here R_d is the radius of the drop, and γ is the surface tension. The δ functions in $p(r)$ and $s(r)$ in Eq. (60) are smeared for better visibility; see text.

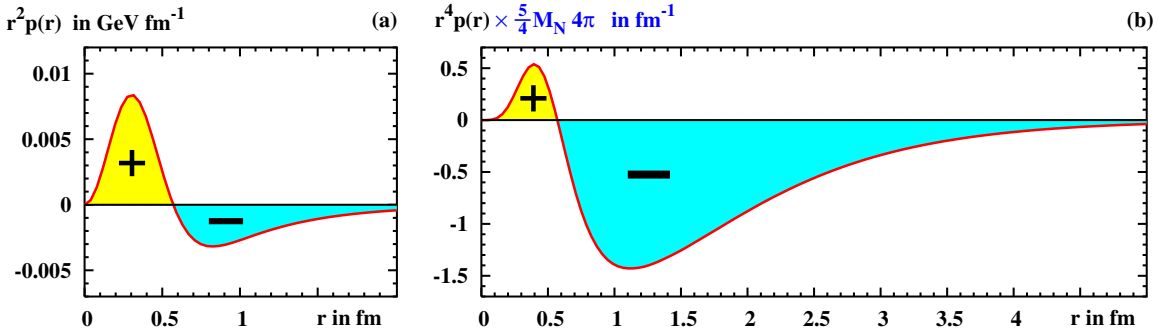

FIG. 4 (color online). (a) $r^2 p(r)$ as a function of r from the CQSM at the physical value of m_π. The shaded regions have—within the numerical accuracy of about half percent—the same surface areas. This shows how the stability condition $\int_0^\infty \mathrm{d}r r^2 p(r) = 0$ in Eq. (57) is realized. (b) The same as (a) but with an additional power of r^2 and the prefactor $5\pi M_N$. Integrating this curve over r yields d_1 according to (17). The plot shows that one obtains a negative sign for d_1 as a consequence of the stability condition (16) shown in Fig. 4(a).

this situation in Fig. 3(c)—where, however, for better visibility the δ functions in (60) are smeared out. This corresponds to allowing the density in the drop to decrease continuously from its constant inner value to zero over a finite "skin" [of the size $\sim \frac{1}{10} R_d$ in Fig. 3(c)].

Comparing the liquid drop picture to the results from the CQSM we observe a remote qualitative similarity. In contrast to the liquid drop, the density "inside" the nucleon is far from being constant, see Fig. 1(a), and one cannot expect the pressure in the nucleon to exhibit a constant plateau as in the liquid drop. Still the pressure exhibits the same qualitative features. The shear forces become maximal in the vicinity of what can be considered as the "edge" of the object. This is the case, in particular, for the liquid drop. However, the edge of the nucleon is far more diffuse, and the distribution of shear forces $s(r)$ is widespread. Of course, the nucleon can hardly be considered a liquid drop. Such an analogy might be more appropriate for nuclei [21]. Nevertheless this comparison gives some intuition on the model results—in particular, about the qualitative shape of the distributions of pressure and shear forces.

Next let us discuss how the stability condition (57) is satisfied. Figure 4(a) shows $r^2 p(r)$ as a function of r. The shaded regions have the same surface areas but opposite sign and cancel each other—within numerical accuracy

$$\int_0^{r_0} \mathrm{d}r r^2 p(r) = 2.61 \text{ MeV}, \qquad \int_{r_0}^{\infty} \mathrm{d}r r^2 p(r) = -2.63 \text{ MeV}. \tag{61}$$

In order to better understand how the soliton acquires stability, it is instructive to look in detail how the total pressure is decomposed of the separate contributions of the discrete level and the continuum contribution. Figure 5 shows that the contribution of the discrete level is always positive. This contribution corresponds in model language to the contribution of the "quark core" and one expects a positive contribution ("repulsion") due to the Pauli principle. At large r the discrete level contribution vanishes exponentially since the discrete level wave-function does so [28].

The continuum contribution is throughout negative—as can be seen from Fig. 5 and can be understood as follows. The continuum contribution can be interpreted as the effect of the pion cloud which in the model is responsible for the forces binding the quarks to form the nucleon, i.e. it provides a negative contribution to the pressure corresponding to attraction. In the chiral limit the continuum contribution exhibits a powerlike decay which dictates the long-distance behavior of the total result for the pressure at large r as follows:

$$p(r) = -\left(\frac{3 g_A}{8\pi f_\pi}\right)^2 \frac{1}{r^6}, \qquad s(r) = 3\left(\frac{3 g_A}{8\pi f_\pi}\right)^2 \frac{1}{r^6}, \tag{62}$$

where for completeness we quote also the result for $s(r)$. For $m_\pi \neq 0$ the continuum contribution exhibits an exponential decay at large r due to the Yukawa tail of the soliton

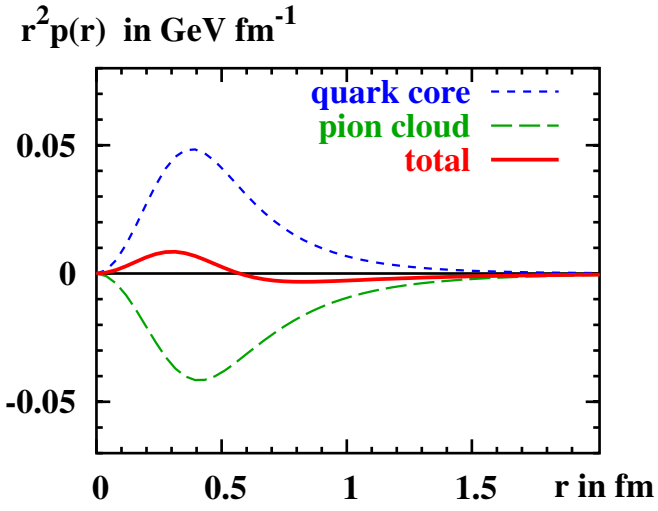

FIG. 5 (color online). The pressure $p(r)$ as a function of r for $m_\pi = 140$ MeV. Dotted line: contribution of the discrete level associated with the quark core. Dashed line: continuum contribution associated with the pion cloud. Solid line: the total result.

profile (29)—like the contribution of the discrete level, however, it still dominates the behavior of the total result. Figure 5 reveals that the actual cancellation between the different contributions leading to (57) are even more impressive than we could guess considering the numbers in Eq. (61). For $m_\pi = 140$ MeV we obtain the following numbers and see that the two contributions cancel each other within numerical accuracy

$$\int_0^\infty dr r^2 p(r)|_{\rm lev} = 26.69 \text{ MeV}, \qquad \int_0^\infty dr r^2 p(r)|_{\rm cont} = -26.71 \text{ MeV}. \tag{63}$$

Finally, we discuss the relation of stability and the sign of the constant d_1. By comparing Figs. 4(a) and 4(b) we immediately understand that in the CQSM the constant d_1 takes a negative value

$$d_1 < 0. \tag{64}$$

This result is presumably of general character. In fact, the observation (64) follows naturally from our intuition on the pressure and shear forces distributions we gained from our study. It seems physically intuitive that in a mechanically stable object the following conditions hold:

(I) for a stable object the pressure has the shape $p(r)\begin{cases} >0 & \text{for } r < r_0 \\ =0 & \text{for } r = r_0 \\ <0 & \text{for } r > r_0 \end{cases}$,

(II) distribution of shear forces satisfies for all r $s(r) > 0$.

From (I) and the stability criterion (16) we conclude that $d_1 \propto \int_0^\infty dr r^4 p(r) < 0$ as illustrated in Figs. 4(a) and 4(b). The same conclusion follows from (II) using $d_1 \propto -\int_0^\infty dr r^4 s(r) < 0$ in (17).

Of course, one can imagine a pressure distribution with more zeros and a different shape than in (I) still yielding (64). However, (I) is the simplest case which one may expect to hold for a ground state—like the nucleon. Such a ground state object is characterized by having one ''surface'' only, although a quite smeared out one in the case of the nucleon, hence the condition (II). A more complicated distribution of the pressure—with more zeros, i.e. also more maxima and minima—would imply an object with several (smeared out) surfaces, which follows from the last condition in Appendix B.

The conjecture (64) is—besides being physically appealing—in agreement with all available information on d_1, see Sec. II. One may therefore suspect that (64) is a general theorem which connects the stability of an object to the sign of its constant d_1. However, such a theorem—if it exists—remains to be rigorously proven for the general case.

VIII. RESULTS FOR THE FORM FACTORS

From the densities $\rho_E(r)$, $\rho_J(r)$, and $p(r)$ which we discussed in detail in Secs. V, VI, and VII, we obtain the form factors of the EMT by means of Eqs. (46)–(48). The results are shown in Fig. 7 for $m_\pi = 0$ and 140 MeV. In the CQSM the form factors $M_2(t)$, $J(t)$ are normalized at $t = 0$ as $M_2(0) = 2J(0) = 1$ as proven in Secs. V and VI. The numerical results satisfy these constraints within a numerical accuracy of (1–2)%; see Figs. 7(a) and 7(b).

In contrast, the normalization of the form factor $d_1(t)$ at $t = 0$ is not known *a priori*. We find $d_1 = d_1(0) < 0$ as anticipated in Sec. VII. The constant d_1 has a well-defined chiral limit. This can be concluded from Eq. (17) which relates d_1 to the distributions of pressure or shear forces, and from the fact that $p(r)$ and $s(r)$ drop off sufficiently fast at large r in the chiral limit; see (62).

The absolute value of d_1 decreases with increasing m_π and we observe a strong sensitivity of d_1 to m_π. That this is not surprising can be understood by considering the chiral expansion of d_1. Expanding $d_1(m_\pi)$ in the model for small m_π we obtain, cf. Appendix I,

$$d_1(m_\pi) = \mathring{d}_1 + \frac{15 g_A^2 M_N}{64\pi f_\pi^2} m_\pi + \ldots \tag{65}$$

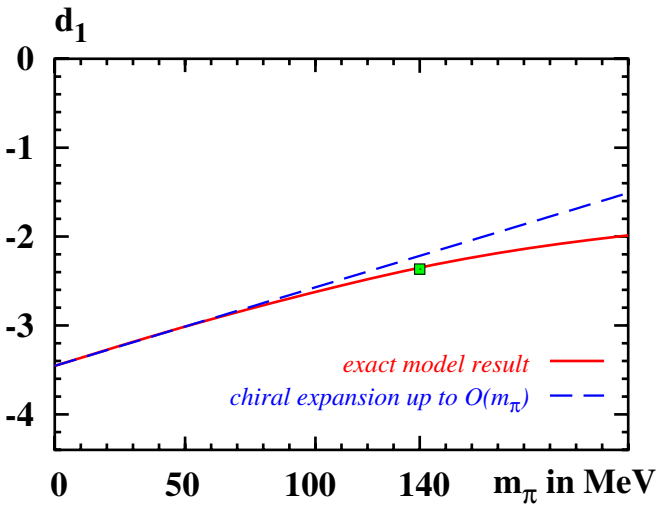

FIG. 6 (color online). The constant d_1 as a function of m_π. Comparison of the full CQSM result, and the expansion of d_1 up the leading nonanalytic term according to Eq. (65). The square marks the physical point.

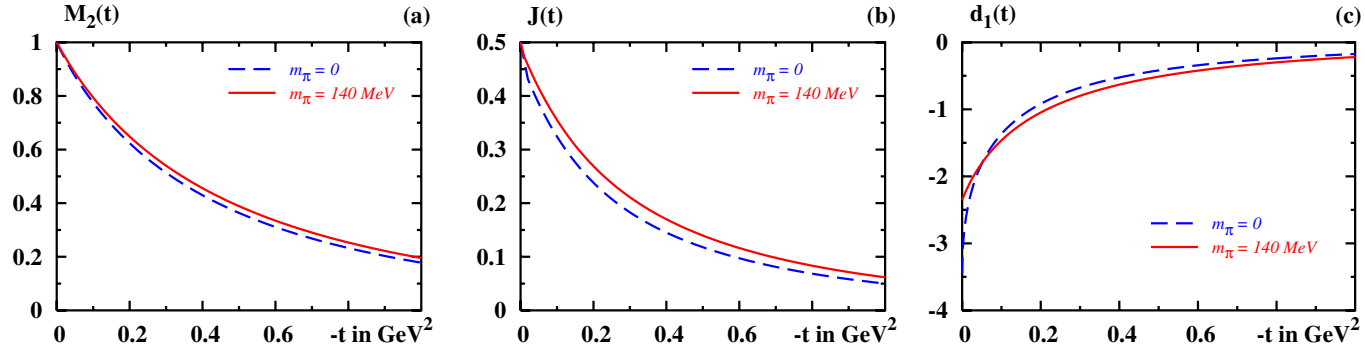

FIG. 7 (color online). The form factors of the energy-momentum tensor $M_2(t)$, $J(t)$, and $d_1(t)$ as functions of t for the pion masses $m_\pi = 0$, 140 MeV. All form factors can be well approximated by dipole fits, however, with the exception of $J(t)$ and $d_1(t)$ in the chiral limit which exhibit infinitely steep slopes at $t = 0$; see text.

Thus, we see that $d_1(m_\pi)$ receives a large leading nonanalytic contribution in the current quark mass $m \propto m_\pi^2$, which is the origin of the strong m_π dependence of $d_1(m_\pi)$. The expansion (65) approximates in the model $d_1(m_\pi)$ to within an accuracy of 15% up to the physical point; see Fig. 6. At the physical point the absolute value of d_1 is reduced by about 30% with respect to its chiral limit value. The numerical results for d_1 are summarized in Table I.

Next, let us focus on the derivatives of the form factors at $t = 0$. From Eq. (11) we conclude that at $t = 0$ the slope of the form factor $M_2(t)$ is given by

$$M_2'(0) = \frac{\langle r_E^2\rangle}{6} + \frac{d_1}{5M_N^2} = \mathring{M}_2'(0) - \frac{21 g_A^2}{128\pi f_\pi^2}\frac{m_\pi}{M_N} + \ldots \tag{66}$$

where the chiral expansion follows from (53) and (65). In particular, $M_2'(0)$ is well defined for all m_π including the chiral limit. The situation is different for the form factors $J(t)$ and $d_1(t)$. The slope of $J(t)$ at $t = 0$ can be deduced from (48) and is given by

$$J'(0) = \frac{\langle r_J^2\rangle}{6} \tag{67}$$

with $\langle r_J^2\rangle$ defined in (56). Since the mean square radius of the angular momentum density diverges in the chiral limit, see Sec. VI, so does $J'(0)$. See also the discussion in Appendix I.

That also the slope of $d_1(t)$ becomes infinitely steep at $t = 0$ can be understood as follows. From Eqs. (11), (14), and (15) it follows that the derivative of $d_1(t)$ at $t = 0$ can be expressed as

$$d_1'(t)|_{t=0} = -\frac{M_N}{42}\int \mathrm{d}^3\mathbf{r} r^4 s(r) = \frac{M_N}{16}\int \mathrm{d}^3\mathbf{r} r^4 p(r). \tag{68}$$

Since in the chiral limit $p(r)$ and $s(r)$ drop off as $\frac{1}{r^6}$ at large r we see that $\mathring{d}_1'(0)$ diverges as $m_\pi \to 0$.

To make this statement more quantitative let us expand $d_1(t)$ in the chiral limit in the model for small t. We obtain

$$\mathring{d}_1(t) = \mathring{d}_1 - \frac{45 g_A^2 M_N}{512 f_\pi^2}\sqrt{-t} + \mathcal{O}(t), \tag{69}$$

which means that in the chiral limit $\mathring{d}_1'(t) \propto 1/\sqrt{-t}$ at small t. Alternatively, one may keep $m_\pi \neq 0$, evaluate the derivative of $d_1(t)$ at $t = 0$, and then consider small m_π. (Note that the limits $m_\pi \to 0$ and $t \to 0$ do not commute.) Then we find that the slope of $d_1(t)$ at $t = 0$ diverges in the chiral limit as

$$\mathring{d}_1'(t)|_{t=0} = -\frac{3 g_A^2 M_N}{32\pi f_\pi^2 m_\pi} + \ldots. \tag{70}$$

The results (69) and (70) are derived in Appendix I. The numerical results for $J(t)$ and $d_1(t)$ in Figs. 7(b) and 7(c) indicate the infinitely steep slopes at $t = 0$ within the numerical accuracy.

Notice that we derived the analytical results in (65), (66), (69), and (70) in the framework of the CQSM. However, the leading nonanalytic terms (i.e. terms $\propto m_\pi$) in the chiral expansion of $d_1(t)$ in (65), (66), (69), and (70) are dictated by chiral symmetry breaking and are *independent* of the details of the chiral theory chosen to derive them. In fact, our results (65), (66), (69), and (70) agree with those obtained from chiral perturbation theory in Ref. [48]—provided one takes into account an important difference. The CQSM is formulated in the large-N_c limit which does not commute with the chiral limit [50]. At large N_c the masses of the nucleon and Δ resonance are degenerated: $M_\Delta - M_N = \mathcal{O}(N_c^{-1})$. Therefore, in the CQSM—in addition to the nucleon considered in chiral perturbation theory [48]—the Δ resonance contributes on equal footing as intermediate state in chiral loops. Considering that in the large N_c limit the pion-Delta-nucleon and pion-nucleon-nucleon couplings are related as $g_{\pi N\Delta} = \frac{3}{2} g_{\pi NN}$ (phenomenologically satisfied to a very good approximation), one finds that the Δ resonance makes a contribution to leading nonanalytic terms which is—for scalar-isoscalar quanti-

ties—2 times larger than that of the nucleon [51]. Hence, our leading nonanalytic terms in Eqs. (65), (66), (69), and (70) are 3 times larger than those obtained from chiral perturbation theory in Ref. [48] where N_c was kept finite.[2] Other examples of the derivation of leading nonanalytic terms in chiral soliton models can be found in [33,51].

Next, we turn to the discussion of the t dependence of the form factors and recall that in the large-N_c limit we strictly speaking are restricted to $|t| \ll M_N^2$. However, in practice it is observed that the CQSM provides reliable results for electromagnetic form factors up to $|t| \lesssim 1$ GeV^2 [30,31].

Figure 7 shows the form factors of the EMT as functions of t for $|t| \leq 1$ GeV^2 for $m_\pi = 0$ and 140 MeV. For $m_\pi \neq 0$ the form factors can be well approximated by dipole fits

$$F(t) = \frac{F(0)}{(1 - t/M_{\rm dip}^2)^2} \tag{71}$$

with the values for the dipole masses quoted in Table I.

It is instructive to compare these results within the model to the electromagnetic form factors—for definiteness we choose the electric form factor of the proton $G_E(t)$ computed in the CQSM in Ref. [30]. Figure 8 shows that $J(t)$ and $G_E(t)$ exhibit a similar t dependence. However, $M_2(t)$ falls off with increasing $|t|$ slower than $G_E(t)$, while $d_1(t)$ shows a faster falloff.

One popular assumption in literature in the context of modelling GPDs is to assume a generic factorized Ansatz of the type $H(x, \xi, t) = H(x, \xi)G(t)$ where $G(t)$ denotes the respective form factor (other approaches are discussed in [17,19,84–87]). This assumption implies that the form factors of the EMT should have approximately the same t dependence as the electromagnetic form factors. Our results indicate that this is quite a rough approximation and support the observations that in the CQSM $H(x, \xi, t) \neq H(x, \xi)G(t)$; see Refs. [17,40]

Let us compare our result for d_1 with the result from direct calculations of GPDs in the model [40] which yield[3] $d_1^Q \approx -8.0$ at the low model scale in the chiral limit. The discrepancy with the corresponding results in Table I is due to the fact that in [40] the momentum-dependent constituent mass $M(p)$ was employed vs our proper-time or Pauli-Villars regularization with $M = \text{const}$, and that the approximative "interpolation formula" was used vs the exact numerical calculation done here.

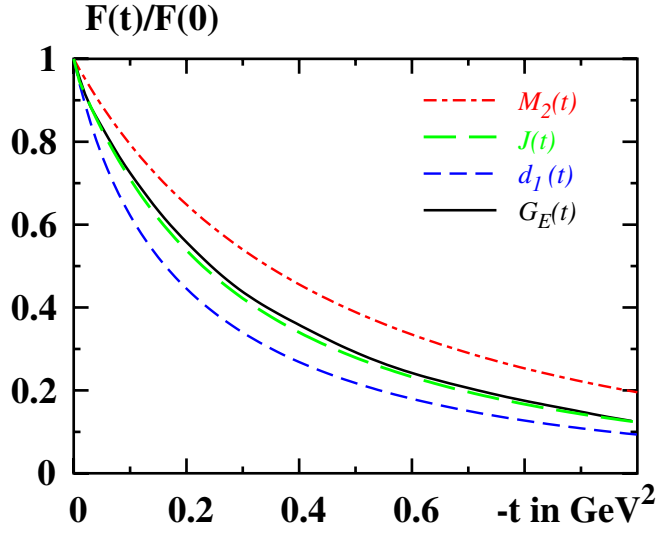

FIG. 8 (color online). EMT form factors as functions of t. Dashed-dotted line: $M_2(t)$. Long-dashed line: $J(t)$. Dashed line: $d_1(t)$; all computed here. Solid line: electric proton form factor $G_E(t)$ from Ref. [30]. All form factors refer to the physical pion mass and are normalized with respect to their values at $t = 0$.

For the mean square radius $\langle r_F^2 \rangle$ of the operator of the EMT trace, see Eqs. (23) and (24), we obtain in the chiral limit

$$\langle \mathring{r}_F^2 \rangle = (1.0\text{–}1.2)\ \text{fm}^2, \tag{72}$$

while its value at the physical point is reduced by about 0.2 fm compared to (72); see Table I. From the chiral expansion of $\langle r_F^2 \rangle$ which follows from Eqs. (24), (53),

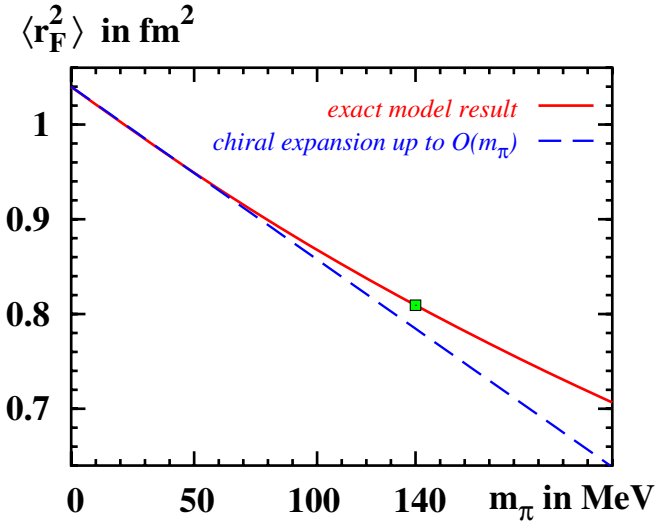

FIG. 9 (color online). Mean square radius of EMT trace operator vs m_π.

[2]Actually, there is one more subtlety to be considered. In the result for the form factor $\frac{4}{5}d_1(t) = C_2(t)$ in Eq. (20) of [48] (see Appendix A for the discussion of the notation) in addition the constant $a_2^{Q,\pi} \equiv M_2^{Q,\pi}$ appears, which describes the fraction of the pion momentum carried by quarks. In the effective theory (25) quarks carry the entire momentum of the pion, i.e. $M_2^{Q,\pi} = 1$ [66].

[3]From this number it was estimated that $d_1 \approx -4.0$ at experimentally relevant scales of few GeV^2 [68] in the following way. The model predicts for the *ratio* $d_1^Q/M_2^Q \approx -8.0$ and experimentally one finds $M_2^Q \approx 0.5$ at scales of few GeV^2. This estimate neglects strictly speaking the different evolution properties of d_1^Q and M^Q which is justified because uncertainties in the model dominate.

and (65) and reads

$$\langle r_F^2\rangle = \langle \mathring{r}_F^2\rangle - \frac{117 g_A^2}{64\pi f_\pi^2 M_N} m_\pi + \ldots, \tag{73}$$

we see that the leading nonanalytic term in (73) explains the main portion of the observed reduction of $\langle r_F^2\rangle$ at the physical point compared to its chiral limit value; see Fig. 9.

It is instructive to compare our result (72) for the mean square radius of the EMT trace to the mean square radius of the traceless part of the EMT $(0.3\ \mathrm{fm})^2$ estimated by means of QCD sum rules [88]. The instanton vacuum model provides a possible explanation why the radius of the trace of the EMT is so much larger than the traceless part. In chiral limit the trace part is basically the gluonic operator $F_{\mu\nu}F^{\mu\nu}$ which is due to one-instanton contributions and appears in leading order in the instanton packing fraction. The traceless part arises from instanton-anti-instanton contributions which appear at subleading order [76].

IX. CONCLUSIONS

In this work we presented a study of the form factors of the EMT in the large-N_c limit in the framework of the CQSM. We provided numerous checks of the theoretical consistency of the model results. Among others, we demonstrated that the same model expressions for the form factors can be derived from the EMT and from GPDs.

We computed the spatial density distributions and mean square radii of the operators of different components of the EMT and its trace. Interesting results are that the energy density related to $\hat{T}^{00}$ in the center of the nucleon is about $1.7\ \mathrm{GeV}^{-3}$, i.e. about 13 times higher than the equilibrium density of nuclear matter. The mean square radius of the operator $\hat{T}^{00}$ is about $0.67\ \mathrm{fm}^2$. For the mean square radius of the ''angular momentum distribution'' related to the operator $\hat{T}^{0k}$ $(k = 1, 2, 3)$ we find a much larger value $1.32\ \mathrm{fm}^2$.

We studied the spatial distribution of strong forces in the nucleon as described in terms of the distributions of pressure and shear forces which are defined by the spatial components $\hat{T}^{jk}$ $(j, k = 1, 2, 3)$ of the EMT. As a by-product of this study we learned how the soliton acquires stability in the CQSM—namely, due to subtle balance of repulsive forces in the center due the ''quark core'' and attractive forces in the outskirts of the nucleon due the ''pion cloud'' which bounds the quarks in the model.

We observed a physically appealing connection between the criterion for the stability of a particle and the sign of the constant d_1, i.e. the form factor $d_1(t)$ at zero-momentum transfer. Our observations imply that for a stable particle one always has $d_1 < 0$, though we cannot prove this conjecture for the general case. All available results for d_1 in literature are compatible with this observation.

We derived the leading nonanalytic chiral contributions to the form factors in the large N_c limit, which agree with results from chiral perturbation theory [47–49] provided one takes into account that the limits $N_c \to \infty$ and $m_\pi \to 0$ do not commute [50,51].

We observed that the model results for the form factors of the EMT can, for $m_\pi > 0$, be well approximated by dipole fits. The different form factors have different t dependences. For $J^Q(t)$ we obtain in the model a dipole mass similar to that of the electromagnetic form factors of the proton. The dipole mass of $M_2(t)$ is much larger than that, while that of $d_1(t)$ is substantially smaller. These results are of interest for the phenomenology of hard exclusive reactions, and, in particular, for the task of extrapolating $J^Q(t)$ to $t = 0$ which is necessary to extract from data information on what portion of the nucleon spin is due to quarks.

Our results yield in the chiral limit for the constant $d_1 = -(3.5\text{–}4.8)$ depending on the regularization and confirm sign and—within model accuracy—magnitude of previous results [40,68]. We observe, however, also a strong m_π dependence of d_1 which is dominated by a sizeable leading nonanalytic (in the current quark mass) contribution proportional to m_π. The latter is responsible for reducing the absolute value of d_1 by about 30% at the physical point compared to its chiral limit value.

We estimated the mean square radius of the EMT trace operator to be about $(1\ \mathrm{fm})^2$ which appears much larger than the corresponding mean square radius of the traceless part of the EMT found to be $(0.3\ \mathrm{fm})^2$ [88] and noticed that the instanton vacuum model provides a possible explanation for that.

A study of the m_π dependence of the EMT form factors in the model at larger values of m_π in the spirit of Ref. [58] and a detailed comparison of the model results to lattice QCD data [52–57] will be presented elsewhere [59].

ACKNOWLEDGMENTS

We thank Pavel Pobylitsa for fruitful discussions and valuable comments. This research is part of the EU integrated infrastructure initiative hadron physics project under Contract No. RII3-CT-2004-506078, and partially supported by the Graduierten-Kolleg Bochum-Dortmund and Verbundforschung of BMBF. D. U. and A. S. acknowledge support from GRICES and DAAD.

Note added.—After this work was completed the work [95] appeared, where in particular the constant d_1 was studied. For d_1^{u+d} similar results were obtained using somehow different model parameters. Interesting is the estimate for the flavor combination d_1^{u-d} which was found rather small and confirms the large-N_c prediction (18).

APPENDIX A: ALTERNATIVE DEFINITION OF FORM FACTORS

The following alternative definition of form factors of the EMT is commonly used in literature, see e.g. [3],

$$\langle p'|\hat{T}^{Q,G}_{\mu\nu}(0)|p\rangle = \bar{u}(p')\Big[A^{Q,G}(t)\frac{\gamma_\mu P_\nu + \gamma_\nu P_\mu}{2} + B^{Q,G}(t) \times \frac{i(P_\mu\sigma_{\nu\rho} + P_\nu\sigma_{\mu\rho})\Delta^\rho}{4M_N} + C^{Q,G}(t) \times \frac{\Delta_\mu\Delta_\nu - g_{\mu\nu}\Delta^2}{M_N} \pm \bar{c}(t)g_{\mu\nu}\Big]u(p). \tag{A1}$$

By means of the Gordon identity $2M_N\bar{u}'\gamma^\alpha u = \bar{u}'(i\sigma^{\alpha\kappa}\Delta_\kappa + 2P^\alpha)u$, Eq. (A1) can be rewritten as Eq. (1) with

$$A^{Q,G}(t) = M_2^{Q,G}(t) \qquad A^{Q,G}(t) + B^{Q,G}(t) = 2J^{Q,G}(t)$$
$$C^{Q,G}(t) = \frac{1}{5}d_1^{Q,G}(t). \tag{A2}$$

The constraints (13) translate in this language into $A^Q(0) + A^G(0) = 1$ and $B^Q(0) + B^G(0) = 0$. The latter constraint means that the total nucleon "gravitomagnetic moment" vanishes.

In models, in which the only dynamical degrees of freedom are effective quark degrees of freedom, the constraint $B^Q(0) = 0$ must hold. Such is the situation in the CQSM where consequently this constraint is satisfied [44].

Interestingly, it was argued [89] that also in QCD the quark and gluon gravitomagnetic moments of the nucleon could vanish separately, i.e. $B^Q(0) = 0$ and $B^G(0) = 0$. That would imply that $M_2^Q(0) = 2J^Q(0)$ and $M_2^G(0) = 2J^G(0)$ at any scale, and not only in the asymptotic limit of a large renormalization scale [3]; see [89] for details.

APPENDIX B: GENERAL RELATIONS FROM THE CONSERVATION OF EMT

Here we collect some worthwhile noticing relations for $p(r)$ and $s(r)$ which can be derived from the differential Eq. (15)—i.e. which follow from the conservation of the EMT.

(i) For *any* $s(r)$ one obtains from (15) a $p(r)$ which *automatically* satisfies the stability condition (16). Therefore, when computing these quantities, for example, in a model, the computation of the pressure is more important and reliable in the sense that the result can be cross-checked by the stability condition (16).

(ii) The pressure at the origin is connected to $s(r)$ by the following integral relation:

$$p(0) = 2\int_0^\infty \mathrm{d}r\frac{s(r)}{r}. \tag{B1}$$

(iii) Assume that $p(r)$ and $s(r)$ vanish at large r faster than any power of r to justify below integration by parts. (In Sec. VII we have seen that this is always the case with the exception of the chiral limit.) Then the following relations hold between the "Mellin moments" of $s(r)$ and $p(r)$:

$$\int_0^\infty \mathrm{d}r r^N s(r) = -\frac{3(N+1)}{2(N-2)}\int_0^\infty \mathrm{d}r r^N p(r) \tag{B2}$$
for $N > -1$,

which are valid also for noninteger values of N. Equation (17) quoted in Sec. II is just a special case of (B2).

(iv) The case $N = 2$ in (B2) has to be treated with care. Taking the limit $N \to 2$ on the right-hand side of (B2) yields—upon use of (16)—the following result:

$$\int_0^\infty \mathrm{d}r r^2 s(r) = -\frac{9}{2}\int_0^\infty \mathrm{d}r r^2(\log r)p(r). \tag{B3}$$

One may worry in which units the "r" in "log$r$" should be provided in (B3). However, this is immaterial due to the stability condition (16).

(v) $p(r)$ and $r^3 s(r)$ exhibit extrema at the same r.

APPENDIX C: CONSERVATION OF EMT IN THE CQSM

In this appendix we demonstrate explicitly that $\langle N'|\partial_\mu\hat{T}^{\mu\nu}_{\mathrm{eff}}|N\rangle = 0$. For that we directly evaluate in the model matrix elements of the operator $\partial_\mu\hat{T}^{\mu\nu}_{\mathrm{eff}}$. For $\partial_0\hat{T}^{0\nu}_{\mathrm{eff}}$ a derivation analog to that yielding (37) and (39) yields immediately

$$\langle N'|\partial_0\hat{T}^{0\nu}_{\mathrm{eff}}|N\rangle = 0. \tag{C1}$$

Hereby one has to consider the cases $\nu = 0$ and $\nu = k$ separately, since the respective model expressions arise from different orders in the $1/N_c$ expansion.

A derivation analog to that yielding (38) gives for matrix elements of the operator $\partial_i\hat{T}^{ik}_{\mathrm{eff}}$ the following result:

$$\langle N'|\partial_i\hat{T}^{ik}_{\mathrm{eff}}|N\rangle = \delta_{S_3'S_3}\frac{M_N N_c}{2}\sum_{n,\mathrm{occ}}\int \mathrm{d}^3\mathbf{x}e^{i\boldsymbol{\Delta}\mathbf{x}}i\nabla^i \times [\phi_n^*\gamma^0\gamma^i(\nabla^k\phi_n) + \phi_n^*\gamma^0\gamma^k(\nabla^i\phi_n) - (\nabla^k\phi_n^*)\gamma^0\gamma^i\phi_n - (\nabla^i\phi_n^*)\gamma^0\gamma^k\phi_n] = \delta_{S_3'S_3}\frac{M_N N_c}{2}\sum_{n,\mathrm{occ}}\int \mathrm{d}^3\mathbf{x}e^{i\boldsymbol{\Delta}\mathbf{x}}(K_1 + K_2) \tag{C2}$$

where

$$K_1 = -\phi_n^*[\nabla^k(-i\gamma^0\gamma^i\nabla^i)\phi_n)] + [-i\gamma^0\gamma^i\nabla^i\phi_n]^*[\nabla^k\phi_n] + (\nabla^k\phi_n^*)(-i\gamma^0\gamma^i\nabla^i\phi_n) - [\nabla^k(-i\gamma^0\gamma^i\phi_n)^*]\phi_n$$
$$K_2 = +i\phi_n^*\gamma^0\gamma^k(\nabla^2\phi_n) - i(\nabla^2\phi_n^*)\gamma^0\gamma^k\phi_n. \tag{C3}$$

From the single-quark equations of motion (26) one obtains the identities $(-i\gamma^0\gamma^i\nabla^i)\phi_n = (E_n - M\gamma^0U^{\gamma_5})\phi_n$ and $(-\nabla^2\phi_n) = (E_n^2 - M^2 - iM\gamma^j(\nabla^j U^{\gamma_5}))\phi_n$ which allow, respectively, to rewrite K_1 and K_2 as follows:

$$K_1 = -K_2 = 2M\phi_n^*\gamma^0(\nabla^k U^{\gamma_5})\phi_n. \tag{C4}$$

Thus, $\langle N'|\partial_i \hat{T}^{ik}_{\rm eff}|N\rangle = 0$ in Eq. (C2). This proves that the form factor $\bar{c}(t)$ in Eq. (1) vanishes in the model. This is consistent since, due to the absence of gluons, in the CQSM the quark part of the EMT must be conserved by itself.

APPENDIX D: REGULARIZATION

The proper-time regularized model expressions for the continuum contributions to the form factors (40)–(42) read

$$M_2(t)_{\rm cont} - \frac{t}{5M_N^2} d_1(t)_{\rm cont} = \frac{N_c}{M_N}\sum_{n,\rm all} R_1(E_n, \Lambda)\langle n|e^{i\mathbf{\Delta}\hat{\mathbf{x}}}|n\rangle, \tag{D1}$$

$$d_1(t)_{\rm cont} = \frac{5M_N N_c}{4t}\sum_{n,\rm all} R_2(E_n, \Lambda)\langle n|\{\gamma^0\boldsymbol{\gamma}\hat{\mathbf{p}}, e^{i\mathbf{\Delta}\hat{\mathbf{x}}}\}|n\rangle, \tag{D2}$$

$$J(t)_{\rm cont} = \frac{iN_c\varepsilon^{klm}\Delta^k}{8It}\sum_{\substack{n,j\ \rm all\\ n\neq j}} R_3(E_n, E_j, \Lambda)\langle n|\tau^l|j\rangle \times\langle j|(\{e^{i\mathbf{\Delta}\hat{\mathbf{x}}}, \hat{p}^m\} + (E_n + E_j)e^{i\mathbf{\Delta}\hat{\mathbf{x}}}\gamma^0\gamma^m)|n\rangle. \tag{D3}$$

The regulator functions R_i appear in the model also in the regularizations of other quantities [31] and are defined as

$$R_1(\omega, \Lambda) = \frac{1}{4\sqrt{\pi}}\int_{1/\Lambda^2}^{\infty}\frac{d\alpha}{\alpha^{3/2}}\exp(-\alpha\omega^2),$$

$$R_2(\omega, \Lambda) = -\frac{1}{2}\frac{\partial}{\partial\omega}R_1(\omega, \Lambda),$$

$$R_3(\omega_1, \omega_2, \Lambda) = \frac{1}{4\sqrt{\pi}}\int_{1/\Lambda^2}^{\infty}d\alpha \times\left[\frac{\exp(-\alpha\omega_1^2) - \exp(-\alpha\omega_2^2)}{\alpha^{3/2}(\omega_2^2 - \omega_1^2)} - \frac{\omega_1\exp(-\alpha\omega_1^2) + \omega_2\exp(-\alpha\omega_2^2)}{\alpha^{1/2}(\omega_1 + \omega_2)}\right]. \tag{D4}$$

That $d_1(t)$ is regularized "differently" in Eqs. (D1) and (D2) is a peculiarity of the proper-time regularization. In the Pauli-Villars regularization all quantities $F = \{M_N, I, M_2(t), J(t), d_1(t)\}$ are regularized in the same way as

$$F_{\rm reg} = F(M) - \frac{M^2}{M_{\rm PV}^2}F(M_{\rm PV}), \tag{D5}$$

where it is understood that the corresponding model expressions are first evaluated with the Hamiltonian (26) and with the Hamiltonian (26) where M replaced by $M_{\rm PV}$, and then finally subtracted according to the prescription (D5).

Notice that for the constraints (50) and (55) to be satisfied by the numerical results it is of crucial importance that $M_2(t)$ and M_N as well as $J(t)$ and I are regularized in the same way. This is the case for both regularizations. In order to make this apparent also for the proper-time regularization we recall that in this method the regularized model expressions for continuum contributions to the nucleon mass (27) and the moment of inertia (30) are given by

$$\begin{aligned} M_{N,\rm cont} &\equiv N_c\sum_{E_n<0}(E_n - E_{n_0})|_{\rm reg} \\ &= N_c\sum_{n,\rm all}(R_1(E_n, \Lambda) - R_1(E_{n_0}, \Lambda)) \\ I_{\rm cont} &\equiv \frac{N_c}{6}\sum_{\substack{E_m>0\\ E_n<0}}\frac{\langle n|\tau^a|m\rangle\langle m|\tau^a|n\rangle}{E_m - E_n}\Bigg|_{\rm reg} \\ &= \frac{N_c}{6}\sum_{\substack{n,m\ \rm all\\ m\neq n}}\langle n|\tau^a|m\rangle\langle m|\tau^a|n\rangle R_3(E_n, E_m, \Lambda). \end{aligned} \tag{D6}$$

Hereby Λ or $M_{\rm PV}$ are fixed to reproduce the physical value of the pion decay constant $f_\pi = 93$ MeV [31]. For $M = 350$ MeV one has $\Lambda = 649$ MeV in the chiral limit, and $\Lambda = 643$ MeV for $m_\pi = 140$ MeV. The proper-time method can, in principle, be applied to any m_π [58]. The Pauli-Villars method can be applied unambiguously in the chiral limit, with $M_{\rm PV} = 556$ MeV reproducing the experimental value of f_π. However, the method meets difficulties in the case of a nonzero current quark mass m [81]. Notice that Λ and $M_{\rm PV}$ are of $\mathcal{O}(\rho^{-1}) \approx 600$ MeV.

APPENDIX E: MODEL EXPRESSIONS FOR $d_1(0)$ AND $d_1'(0)$ FROM THE EMT

One consequence of the conservation of the EMT, see Sec. II and Appendices B and C, is that there are two different expressions for $d_1(t)$. In one $d_1(t)$ is related to $p(r)$ and in the other to $s(r)$. Both are, of course, equivalent. However, this is not obvious from the explicit model expressions.

Here we derive model expressions for $d_1(0)$ and $d_1'(0)$ from the EMT in terms of $p(r)$ and $s(r)$ which will be useful below for the explicit demonstration that the expressions for $d_1(t)$ obtained from the EMT and GPDs are equivalent.

The model expression for the spatial components of the static energy-momentum tensor (8) reads

$$T^{kl}(\mathbf{r}) = \frac{N_c}{4i}\sum_{n,\rm occ}\phi_n^*(\mathbf{r})(-\gamma^0\gamma^k\overleftarrow{\nabla}^l + \gamma^0\gamma^k\vec{\nabla}^l + (k\leftrightarrow l))\phi_n(\mathbf{r}). \tag{E1}$$

For the model expressions for the form factor $d_1(t)$ and its derivative at $t = 0$ we obtain

$$d_1(0) = \frac{5N_cM_N}{4}\sum_{n,\mathrm{occ}}\langle n|\{\gamma^0\boldsymbol{\gamma}\hat{\mathbf{p}},\hat{\mathbf{r}}^2\}|n\rangle$$
$$= -\frac{N_cM_N}{4}\sum_{n,\mathrm{occ}}\left\langle n\left|\left\{\gamma^0\gamma^k\hat{p}^l,\left(\hat{r}^k\hat{r}^l-\frac{\hat{\mathbf{r}}^2}{3}\delta^{kl}\right)\right\}\right|n\right\rangle, \tag{E2}$$

$$d_1'(0) = \frac{N_cM_N}{96}\sum_{n,\mathrm{occ}}\langle n|\{\gamma^0\boldsymbol{\gamma}\hat{\mathbf{p}},\hat{\mathbf{r}}^4\}|n\rangle$$
$$= -\frac{N_cM_N}{56}\sum_{n,\mathrm{occ}}\left\langle n\left|\left\{\gamma^0\gamma^k\hat{p}^l,\left(\hat{r}^k\hat{r}^l-\frac{\hat{\mathbf{r}}^2}{3}\delta^{kl}\right)\hat{\mathbf{r}}^2\right\}\right|n\right\rangle. \tag{E3}$$

The first relations in (E2) and (E3) are more practical for a numerical evaluation. They follow, for example, from taking the limit $\Delta^i \to 0$ in (41) and making use of (16) and hedgehog symmetry. Notice, that (E2) can alternatively be derived from (17) and (44)—which is a cross check for the intermediate model expressions.

In order to find the equivalent second relations in (E2) and (E3), we inspect Eq. (9) for small momentum transfers using for $T^{ij}(\mathbf{r})$ the model expression in (E1). This yields

$$d_1(0)+t\frac{7}{3}d_1'(0)+\mathcal{O}(t^2) = -\frac{N_cM_N}{4}\sum_{n,\mathrm{occ}}\left\langle n\left|\left\{\gamma^0\gamma^i\hat{p}^j,\left(\hat{r}^i\hat{r}^j-\frac{\hat{\mathbf{r}}^2}{3}\delta^{ij}\right)\times\left(1+\frac{\hat{\mathbf{r}}^2t}{6}+\mathcal{O}(t^2)\right)\right\}\right|n\right\rangle, \tag{E4}$$

from which we read off the desired results. The second relation in (E3) follows also immediately from (13) and (E1).

Comparing (E1) with the general relations for $p(r)$ and $s(r)$ with $T^{ij}(r)$,

$$p(r) = \frac{1}{3}T^{ij}(r)\delta^{ij}, \qquad s(r) = \frac{3}{2}T^{ij}(r)\left(\frac{r^ir^j}{r^2}-\frac{1}{3}\delta^{ij}\right), \tag{E5}$$

we recognize that (E2) is just Eq. (17) in the model, while (E3) is the model version of Eq. (68).

APPENDIX F: POLYNOMIALITY OF $(H^u + H^d)\times(x, \xi, t)$ AT $t \neq 0$

The expression for $(H^u + H^d)(x, \xi, t)$, which in the SU(2) version of the CQSM already exhausts the sum over quark flavors in Eq. (3), was derived, evaluated, and discussed in [40]. With the lightlike vector n in Eq. (2) chosen to be $n^\mu \propto (1, 0, 0, -1)$ the model expression is given by

$$(H^u+H^d)(x,\xi,t) = M_NN_c\int\frac{dz^0}{2\pi}\sum_{n,\mathrm{occ}}e^{iz^0(xM_N-E_n)}\times\left\langle n\left|(1+\gamma^0\gamma^3)\exp\left(-i\frac{z^0}{2}\hat{p}^3\right)\times\exp(i\boldsymbol{\Delta}\hat{\mathbf{x}})\exp\left(-i\frac{z^0}{2}\hat{p}^3\right)\right|n\right\rangle. \tag{F1}$$

The study of Ref. [40] was supplemented in [42] by the explicit proof that $(H^u + H^d)(x, \xi, t)$ in the model satisfies the polynomiality condition (5) at $t = 0$. In this appendix we generalize the proof of Ref. [42] to $t \neq 0$.

The reason why the proof of [42] was restricted to the case $t = 0$ is connected to the fact that the information on ξ and t on the right-hand side of Eq. (F1) is *implicitly* encoded in the 3-vector $\boldsymbol{\Delta}$. In the large-N_c kinematics $\Delta^3 = -2\xi M_N$ and $t = -\boldsymbol{\Delta}^2$. By keeping $\xi \neq 0$ and continuing analytically the moments of $(H^u + H^d)(x, \xi, t)$ to the point $t = 0$, one obtains model expressions depending on ξ only. That simplifies the situation considerably [42].

However, the proof of [42] can be generalized to $t \neq 0$ by using the following remarkable identity

$$\exp(i\boldsymbol{\Delta}\mathbf{x}) = \sum_{l=0}^{\infty}i^l(2l+1)j_l(r\sqrt{-t})P_l(\cos\theta)\times P_l\left(-\frac{2\xi M_N}{\sqrt{-t}}\right), \tag{F2}$$

where $r = |\mathbf{x}|$ and $\cos\theta = x^3/|\mathbf{x}|$ and $j_l(z)$ and $P_l(z)$ denote, respectively, Bessel functions and Legendre polynomials. As a by-product we remark that by inserting the identity (F2) in (F1) we see *explicitly* that $(H^u + H^d)\times(x, \xi, t)$ is a function only of ξ and t (and x, of course) but not of the 3-vector $\boldsymbol{\Delta}$.

The identity (F2) can be derived as follows. We rewrite the 3-vector $\boldsymbol{\Delta}$ as $\boldsymbol{\Delta} = (\sin\delta\cos\alpha, \sin\delta\sin\alpha, \cos\delta)\sqrt{-t}$ where $\cos\delta = -2\xi M_N/\sqrt{-t}$ and $\alpha \in [0; 2\pi]$ describes the orientation of $\boldsymbol{\Delta}$ in the plane perpendicular to the spatial direction of the light-cone. Then, by using spherical coordinates for $\mathbf{x}$, we obtain

$$\exp(i\boldsymbol{\Delta}\mathbf{x}) = \sum_{l=0}^{\infty}i^l(2l+1)j_l(r\sqrt{-t})P_l(\cos\theta\cos\delta + \sin\theta\sin\delta\cos(\alpha-\phi)). \tag{F3}$$

Next we rewrite the Legendre polynomials using the addition theorem as

$$P_l(\cos\theta\cos\delta+\sin\theta\sin\delta\cos(\alpha-\phi)) = P_l(\cos\theta)P_l(\cos\delta) + 2\sum_{j=1}^{l}\frac{(l-j)!}{(l+j)!}P_l^j(\cos\theta)P_l^j(\cos\delta)\cos(l(\alpha-\phi)). \tag{F4}$$

The physical process described by the GPD does not depend on the orientation of $\boldsymbol{\Delta}$ in the transverse plane. This is reflected by the fact that the matrix elements in (F1) are independent of α. (Changes of α can be compensated by appropriate hedgehog rotations.) Thus, we can eliminate the artificial dependence on α—for example by averaging the matrix elements in (F1) over α. The latter is equivalent to taking the average over α in (F4). Inserting the result into (F3) gives finally the identity (F2).

Notice that for $\epsilon \to 0$ the product $(2l+1) j_l(A\epsilon) P_l(B/\epsilon) \to (AB)^l/l! + \mathcal{O}(\epsilon^2)$. Thus, taking the limit $t \to 0$ while keeping $\xi \neq 0$ in (F2) yields

$$\lim_{\substack{\text{analytical}\\ \text{continuation}\\ t\to 0, \xi\neq 0}} \exp(i\boldsymbol{\Delta}\mathbf{x}) = \sum_{l=0}^{\infty} \frac{(-i2\xi M_N|\mathbf{x}|)^l}{l!} P_l(\cos\theta), \tag{F5}$$

reproducing Eq. (20) of Ref. [42] which was derived independently in a different way.

The proof of polynomiality at $t = 0$ given in Ref. [42] is generalized to any $t \neq 0$ by replacing Eq. (20) in [42] by our more general identity (F2) and repeating literally the steps done in Eqs. (21–28) in [42]. This yields

$$\int \mathrm{d}x x^{m-1}(H^u + H^d)(x,\xi,t) = \frac{N_c}{M_N^{m-1}} \sum_{n,\mathrm{occ}} \sum_{k=0}^{m-1} \binom{m-1}{k} \frac{E_n^{m-1-k}}{2^k} \sum_{l=0,2,4,\ldots}^{k+1} i^l (2l+1) P_l\!\left(\frac{2\xi M_N}{\sqrt{-t}}\right) \sum_{j=0}^{k} \binom{k}{j} \langle n|(\gamma^0\gamma^3)^k \times (\hat{p}^3)^j j_l(|\hat{\mathbf{x}}|\sqrt{-t}) P_l(\cos\hat{\theta}) (\hat{p}^3)^{k-j}|n\rangle, \tag{F6}$$

and explicitly demonstrates that the model expression (F1) does satisfy the polynomiality property for any $t \neq 0$. Note that this includes also positive t allowing one to study in principle the region of timelike momentum transfers, where GPDs "become" nucleon-antinucleon distribution amplitudes [90,91].

APPENDIX G: $M_2(t)$ AND $d_1(t)$ FROM GPDS

In this and the following appendix we introduce labels to distinguish the model expressions for form factors derived from GPDs and EMT—with the aim to prove finally that they are equivalent. From Eq. (F6) we read off the model expressions for the second Mellin moment of $(H^u + H^d)(x,\xi,t)$, see Eq. (3),

$$\begin{aligned} M_2(t)|_{\mathrm{GPD}} &= \frac{N_c}{M_N} \sum_{n,\mathrm{occ}} \langle n|E_n j_0(|\hat{\mathbf{x}}|\sqrt{-t})|n\rangle + \frac{N_c}{2M_N} \sum_{n,\mathrm{occ}} \left\langle n \left| \left[\left\{ \gamma^0\gamma^3\hat{p}^3, j_0(|\hat{\mathbf{x}}|\sqrt{-t}) + \frac{5}{2} j_2(|\hat{\mathbf{x}}|\sqrt{-t}) P_2(\cos\hat{\theta}) \right\} \right] \right| n \right\rangle, \\ d_1(t)|_{\mathrm{GPD}} &= \frac{75 N_c M_N}{4t} \sum_{n,\mathrm{occ}} \langle n|\{\gamma^0\gamma^3\hat{p}^3, j_2(|\hat{\mathbf{x}}|\sqrt{-t}) P_2(\cos\hat{\theta})\}|n\rangle. \end{aligned} \tag{G1}$$

By comparing the expressions for $M_2(t)|_{\mathrm{GPD}}$ and $d_1(t)|_{\mathrm{GPD}}$ in (G1), and by exploring hedgehog symmetry we observe

$$\begin{aligned} \frac{5N_c}{4M_N} \sum_{n,\mathrm{occ}} \langle n|\{\gamma^0\gamma^3\hat{p}^3, j_2(|\hat{\mathbf{x}}|\sqrt{-t}) P_2(\cos\hat{\theta})\}|n\rangle &= \frac{t}{15M_N^2} d_1(t)_{\mathrm{GPD}} \\ \frac{N_c}{M_N} \sum_{n,\mathrm{occ}} \langle n|E_n j_0(|\hat{\mathbf{x}}|\sqrt{-t})|n\rangle = \frac{N_c}{M_N} \sum_{n,\mathrm{occ}} \langle n|E_n e^{i\boldsymbol{\Delta}\hat{\mathbf{x}}}|n\rangle &\equiv \left[M_2(t) - \frac{t}{5M_N^2} d_1(t) \right]_{\mathrm{EMT}} \\ \frac{N_c}{2M_N} \sum_{n,\mathrm{occ}} \langle n|\{\gamma^0\gamma^3\hat{p}^3, j_0(|\hat{\mathbf{x}}|\sqrt{-t})\}|n\rangle = \frac{N_c}{6M_N} \sum_{n,\mathrm{occ}} \langle n|\{\gamma^0\boldsymbol{\gamma}\hat{\mathbf{p}}, e^{i\boldsymbol{\Delta}\hat{\mathbf{x}}}\}|n\rangle &\equiv \frac{2t}{15M_N^2} d_1(t)_{\mathrm{EMT}}. \end{aligned} \tag{G2}$$

Thus, Eq. (G1) states that

$$\left[M_2(t) - \frac{t}{15M_N^2} d_1(t) \right]_{\mathrm{GPD}} = \left[M_2(t) - \frac{t}{15M_N^2} d_1(t) \right]_{\mathrm{EMT}}. \tag{G3}$$

This means that the model expressions from GPDs and from EMT are equivalent for this particular linear combination of $M_2(t)$ and $d_1(t)$. In order to prove that this is true also for the separate form factors we have to show explicitly that e.g. one can derive the same model expression for $d_1(t)_{\mathrm{GPD}}$ from the EMT. One way to do this is to demonstrate that $d_1(t)_{\mathrm{GPD}}$ satisfies the differential Eq. (10) *derived from the EMT* with appropriate boundary conditions.

For that let us first remove the preference of the 3-axis from the expression for $d_1(t)|_{\mathrm{GPD}}$ in (G1) which is due to arbitrarily choosing the lightlike vector $n^\mu \propto (1,0,0,-1)$; see above. We remove this arbitrariness by averaging the expression (G1) over directions. This yields

$$\langle\{\gamma^0\gamma^3\hat{p}^3, P_2(\cos\hat{\theta})j_2(|\hat{\mathbf{x}}|\sqrt{-t})\}\rangle_{\rm av} = \frac{1}{5}\left\{\gamma^0\gamma^k\hat{p}^l, \left(\hat{x}^l\hat{x}^k - \frac{1}{3}|\hat{\mathbf{x}}|^2\delta^{kl}\right)\frac{j_2(|\hat{\mathbf{x}}|\sqrt{-t})}{|\hat{\mathbf{x}}|^2}\right\}, \quad \text{(G4)}$$

and using the identity

$$\left(1 + \frac{4t}{3}\frac{\mathrm{d}}{\mathrm{d}t} + \frac{4t^2}{15}\frac{\mathrm{d}^2}{\mathrm{d}t^2}\right)\frac{j_2(|\hat{\mathbf{x}}|\sqrt{-t})}{|\hat{\mathbf{x}}|^2(-t)} = \frac{j_0(|\hat{\mathbf{x}}|\sqrt{-t})}{15} \quad \text{(G5)}$$

we see that $d_1(t)_{\rm GPD}$ satisfies the differential Eq. (10)

$$\left[d_1(t) + \frac{4t}{3}d_1'(t) + \frac{4t^2}{15}d_1''(t)\right]_{\rm GPD} = -\frac{N_cM_N}{4}\sum_{n,\rm occ}\left\langle n\left|\left\{\gamma^0\gamma^k\hat{p}^l, \left(\hat{x}^l\hat{x}^k - \frac{1}{3}|\hat{\mathbf{x}}|^2\delta^{kl}\right)\right.\right.\right.$$
$$\left.\left.\left.\times\, j_0(|\hat{\mathbf{x}}|\sqrt{-t})\right\}\right|n\right\rangle \equiv -\frac{M_N}{2}\int \mathrm{d}^3\mathbf{r}e^{-i\mathbf{r}\boldsymbol{\Delta}}T^Q_{ij}(\mathbf{r})\left(r^ir^j - \frac{\mathbf{r}^2}{3}\delta^{ij}\right). \quad \text{(G6)}$$

Next, using (G4) and expanding the expression for $d_1(t)_{\rm GPD}$ in (G1) we obtain

$$d_1(0)|_{\rm GPD} = -\frac{N_cM_N}{4}\sum_{n,\rm occ}\left\langle n\left|\left\{\gamma^0\gamma^k\hat{p}^l, \left(\hat{x}^l\hat{x}^k - \frac{1}{3}|\hat{\mathbf{x}}|^2\delta^{kl}\right)\right\}\right|n\right\rangle$$
$$d_1'(0)|_{\rm GPD} = -\frac{N_cM_N}{56}\sum_{n,\rm occ}\left\langle n\left|\left\{\gamma^0\gamma^k\hat{p}^l, \left(\hat{x}^l\hat{x}^k - \frac{1}{3}|\hat{\mathbf{x}}|^2\delta^{kl}\right)|\hat{\mathbf{x}}|^2\right\}\right|n\right\rangle, \quad \text{(G7)}$$

which coincides with the expressions obtained from the EMT in Eqs. (E2) and (E3). This completes the proof that one obtains the same model expressions for the form factors $d_1(t)$ and $M_2(t)$ from GPDs and from the EMT.

APPENDIX H: $J(t)$ FROM GPDS

Here we show that the model expression for $J(t)_{\rm EMT}$ obtained from the EMT in Eq. (42) coincides with the model expression for $J(t)_{\rm GPD}$ which results from GPDs [3] by adding up the sum rules (3) and (4).

The model expression for $(H^u + H^d + E^u + E^d)\times(x, \xi, t)$, which we shall refer to as $E_M(x, \xi, t)$ for brevity, reads [44]

$$E_M(x,\xi,t) = \frac{iM_N^2N_c}{2I}\frac{\epsilon^{3ab}\Delta^a}{\boldsymbol{\Delta}_\perp^2}\int\frac{\mathrm{d}z^0}{2\pi}e^{iz^0xM_N}\left[\left\{\sum_{\substack{m,\rm occ\\ j,\rm all}}e^{-iz^0E_m} - \sum_{\substack{m,\rm all\\ j,\rm occ}}e^{-iz^0E_j}\right\}\frac{1}{E_m - E_j}\langle m|\tau^b|j\rangle\langle j|(1+\gamma^0\gamma^3)\exp(-iz^0\hat{p}^3/2)\right.$$
$$\times\exp(i\boldsymbol{\Delta}\hat{\mathbf{X}})\exp(-iz^0\hat{p}^3/2)|m\rangle + iz^0\sum_{m,\rm occ}e^{-iz^0E_m}\langle m|\tau^b(1+\gamma^0\gamma^3)\exp(-iz^0\hat{p}^3/2)$$
$$\left.\times\exp(i\boldsymbol{\Delta}\hat{\mathbf{X}})\exp(-iz^0\hat{p}^3/2)|m\rangle\right]. \quad \text{(H1)}$$

Integrating the $xE_M(x, \xi, t)$ over x yields, after substituting $x \to y = xM_N$ and extending the limits of y integration to the entire y axis which is justified in the large N_c limit due to $M_N = \mathcal{O}(N_c)$, the following result:

$$\int_{-1}^{1}\mathrm{d}xxE_M(x,\xi,t) = \frac{iN_c}{2I}\frac{\epsilon^{3ab}\Delta^a}{\boldsymbol{\Delta}_\perp^2}\left[\left\{\sum_{\substack{m,\rm occ\\ j,\rm all}}E_m - \sum_{\substack{m,\rm all\\ j,\rm occ}}E_j\right\}\frac{1}{E_m - E_j}\langle m|\tau^b|j\rangle\langle j|(1+\gamma^0\gamma^3)\exp(i\boldsymbol{\Delta}\hat{\mathbf{X}})|m\rangle + \frac{1}{2}\left\{\sum_{\substack{m,\rm occ\\ j,\rm all}} - \sum_{\substack{m,\rm all\\ j,\rm occ}}\right\}\right.$$
$$\left.\times\frac{1}{E_m - E_j}\langle m|\tau^b|j\rangle\langle j|(1+\gamma^0\gamma^3)\{\hat{p}^3, \exp(i\boldsymbol{\Delta}\hat{\mathbf{X}})\}|m\rangle - \sum_{m,\rm occ}\langle m|\tau^b(1+\gamma^0\gamma^3)\exp(i\boldsymbol{\Delta}\hat{\mathbf{X}})|m\rangle\right]. \quad \text{(H2)}$$

Consider the unitary transformation $G_5 \equiv \gamma^2\gamma^5\tau^2$ in the notation of [92] with the properties $G_5\gamma^\mu G_5^{-1} = (\gamma^\mu)^T$ and $G_5\tau^aG_5^{-1} = -(\tau^a)^T$. It transforms in coordinate space the Hamiltonian (26) and its eigenstates as $G_5HG_5^{-1} = H^T$ and $G_5\Phi_n(\mathbf{x}) = \Phi_n^*(\mathbf{x})$. Making use of this transformation we obtain the identities

$$\begin{aligned}\langle j|\tau^b|m\rangle &= \langle m|(-\tau^b)|j\rangle,\\ \langle j|(1+\gamma^0\gamma^3)\exp(i\boldsymbol{\Delta}\hat{\mathbf{X}})|m\rangle &= \langle m|(1-\gamma^0\gamma^3)\exp(i\boldsymbol{\Delta}\hat{\mathbf{X}})|j\rangle,\\ \langle j|\tau^b(1+\gamma^0\gamma^3)\exp(i\boldsymbol{\Delta}\hat{\mathbf{X}})|m\rangle &= \langle m|\tau^b(-1+\gamma^0\gamma^3)\exp(i\boldsymbol{\Delta}\hat{\mathbf{X}})|j\rangle,\\ \langle j|(1+\gamma^0\gamma^3)\{\hat{p}^3, \exp(i\boldsymbol{\Delta}\hat{\mathbf{X}})\}|m\rangle &= \langle m|(1-\gamma^0\gamma^3)\{-\hat{p}^3, \exp(i\boldsymbol{\Delta}\hat{\mathbf{X}})\}|j\rangle.\end{aligned} \quad \text{(H3)}$$

One obtains

$$\int_{-1}^{1}\mathrm{d}xxE_M(x,\xi,t) = \frac{iN_c}{2I}\frac{1}{\boldsymbol{\Delta}_\perp^2}\sum_{\substack{m,\rm occ\\ j,\rm non}}F_{mj} \quad \text{(H4)}$$

with

$$F_{mj} = \frac{\epsilon^{ab3}\Delta^a}{E_m - E_j}\langle m|\tau^b|j\rangle\langle j|[\gamma^0\gamma^3(E_m + E_j)\exp(i\boldsymbol{\Delta}\hat{\mathbf{X}}) + \{\hat{p}^3, \exp(i\boldsymbol{\Delta}\hat{\mathbf{X}})\}]|m\rangle$$
$$= \frac{1}{3}\frac{\epsilon^{abc}\Delta^a}{E_m - E_j}\langle m|\tau^b|j\rangle\langle j|[\gamma^0\gamma^c(E_m + E_j)\exp(i\boldsymbol{\Delta}\hat{\mathbf{X}}) + \{\hat{p}^c, \exp(i\boldsymbol{\Delta}\hat{\mathbf{X}})\}]|m\rangle, \tag{H5}$$

where in the second step we made use of the hedgehog symmetry. The final step necessary to recognize that (H4) and (H5) coincide with the expression (42) is the following. Notice that in the expression in Eqs. (H4) and (H5) there is no more reference to the 3-direction which was picked out by arbitrarily choosing the space direction of light-cone vector n^μ along the 3-axis. Therefore, it is justified to identify $\boldsymbol{\Delta}_\perp^2 = \frac{2}{3}\boldsymbol{\Delta}^2 = -\frac{2}{3}t$, which finally leads us to the result

$$2J(t)_{\rm GPD} \equiv \int_{-1}^{1} {\rm d}x x E_M(x,\xi,t) \equiv 2J(t)_{\rm EMT}. \tag{H6}$$

APPENDIX I: CHIRAL PROPERTIES OF THE FORM FACTORS

In this appendix we study the chiral properties of the EMT form factors and start with $d_1(t)$ because here we face simpler expressions and the method is more easily explained. We start from the expression (G1) for $d_1(t)$, and rewrite its continuum contribution in terms of the Feynman propagator, see Appendix A of Ref. [34], and expand it in gradients of the U field. In leading order of this expansion we obtain

$$d_1(t)_{\rm cont} = \frac{75 f_\pi^2 M_N}{4t}\int {\rm d}^3\mathbf{x}\, j_2(r\sqrt{-t})P_2(\cos\theta)\,{\rm tr}_{\rm F}[\nabla^3 U]\times[\nabla^3 U^\dagger] + \ldots, \tag{I1}$$

where the dots denote terms containing three or more gradients of the U field. Taking $t \to 0$ in (I1), and using $j_l(z) = \frac{z^l}{(2l+1)!!} + \mathcal{O}(z^{l+2})$ for $z \ll 1$, we recover the result for $d_1^{\rm cont}$ in Eq. (44) of Ref. [42].[4]

[4]In [42] in the leading order in gradient expansion it was estimated $d_{1,\rm grad}^{\rm LO\,cont} \approx -9.46$ to be compared to $d_{1,\rm exact}^{\rm cont} = -8.34$ which is the exact result obtained here in proper-time regularization, i.e. also in this case the gradient expansion provides a useful estimate for the continuum contribution of a quantity. Let us take here the opportunity to correct an error in [42]. The level contribution to d_1 is not zero—contrary to the claim in Eq. (43) of [42]. Instead, it is $d_1^{\rm lev} = 4.88$ with the self-consistent proper-time profile. In fact, the level contribution to d_1 (and to the pressure) cannot be zero. It plays a crucial role in establishing the stability of the soliton, see Sec. VII. We stress that reliable results which satisfy the stability condition and all other requirements can only be obtained from evaluating numerically the exact model expressions, with the correct self-consistent profile; see Sec. VII.

The result in Eq. (I1) can be used to study the chiral properties of $d_1(t)$. For that the leading large-r (long-distance) behavior of the integrand in (I1) plays the crucial role. Therefore, for this purpose it is legitimate to neglect both, the discrete level contribution which has exponential falloff at large r and higher order terms in the gradient expansion which have additional power suppression with respect to the leading order term in (I1).

In Eq. (G1) we have chosen as a starting point the expression $d_1(t)$ in terms of $s(r)$; see Appendix G. Therefore—after taking the flavor-trace ${\rm tr}_{\rm F}$ in (I1), integrating out the angular dependence, restoring the integral over the full solid angle, and comparing to Eq. (17)—we read off the expression for $s(r)$,

$$d_1(t)_{\rm cont} = \frac{5M_N}{t}\int {\rm d}^3\mathbf{x}\, j_2(r\sqrt{-t})s(r) \quad \text{with}$$
$$s(r) = f_\pi^2\left(P'(r)^2 - \frac{\sin^2 P(r)}{r^2}\right) + \ldots \tag{I2}$$

Making use of the long-distance behavior of the profile (29) we obtain for the large-r behavior of $s(r)$ in the chiral limit the result quoted in Eq. (62). The large-r behavior of $p(r)$ quoted there follows from (15).

In order to derive the leading nonanalytic contributions to $d_1(t)$ we choose to work with the following analytic form of the soliton profile

$$P(r) = -2\arctan\left[\frac{R^2}{r^2}(1 + m_\pi r)\exp(-m_\pi r)\right]. \tag{I3}$$

This profile was demonstrated to be a good approximation to the true self-consistent profile [28]. Since it does not correspond to the true minimum of the soliton energy, e.g., the approximate result for the pressure obtained with this profile does not satisfy the stability condition (16). However, all that matters for our purposes is that it exhibits the correct chiral behavior; see (29). The "soliton radius" R in (I3) is connected to the constant A in (29) by $A = 2R^2$.

Let us focus on the chiral expansion of $d_1(t)_{\rm cont}$ at zero-momentum transfer. We obtain

$$d_1^{\rm cont} = -\frac{4\pi}{3} f_\pi^2 M_N R^3 G(m_\pi R);$$
$$G(a) = \int_0^\infty {\rm d}z \frac{4z^6(3 + 6az + 7a^2z^2 + 4a^3z^3 + a^4z^4)e^{-2az}}{(z^4 + (1 + az)^2 e^{-2az})^2}. \tag{I4}$$

The zeroth order in the Taylor series of the function $G(a)$ around $a = 0$ is $G(0) = \int_0^\infty {\rm d}z 12z^6/(z^4 + 1)^2 = 9\pi/\sqrt{8}$.

To find the linear term in the Taylor expansion of $G(a)$, we proceed as follows, c.f. Appendix B of [33] for a similar calculation. We consider $G'(a)$ at $a \neq 0$, substitute $z \to y = az$, and consider then the limit $a \to 0$. Notice that had we decided to evaluate (I4) in a finite volume, let us say in a spherical box of radius D, then the upper limit of the y integration would be Dm_π. Thus, before taking the chiral

limit it is crucial to take first the infinite volume limit $D \to \infty$ [33], as these two limits do not commute. This yields $G'(a)|_{a=0} = -8 \int_0^\infty dy(-1 + y + 2y^2 + y^3)e^{-2y} = -5$. Thus, we obtain

$$G(a) = G(0) - 5a + \text{higher order terms in a.} \qquad \text{(I5)}$$

Inserting this result in (I4) we reproduce the chiral limit result in Eq. (46) of [42] which, however, provides just one contribution to the chiral limit value of d_1. Other contributions are of importance; see Footnote 4.

The situation is different for the linear m_π correction to d_1. As explained above, here the expansion (I5) provides, in fact, the correct leading nonanalytic term in the chiral expansion of the full expression for d_1 in the model. Combining (I4) and (I5) and eliminating $R \equiv \sqrt{A/2}$ in favor of g_A and f_π according to (29) we obtain Eq. (65). The result for $d_1'(0)$ in (70) is obtained similarly.

To derive the small t expansion of $d_1(t)$ in the chiral limit in Eq. (69) one can integrate (I2) exactly. The result is a bulky and not illuminating expression which we do not quote here. Expanding it for small t yields (69).

Let us turn to the discussion of the form factor $M_2(t)$. At $t = 0$ we have for all m_π exactly $M_2(0) = 1$; see Eq. (50). The slope of $M_2(t)$ at zero-momentum transfer, however, has a nontrivial chiral expansion. Because of (66) we need for that the chiral expansion of $d_1(t)$, see above, and that of the mean square radius of the energy density. In the above described way we obtain from the expression (52) for the energy density in the leading order gradient expansion the following contribution:

$$\langle r_E^2 \rangle_{\text{part 1}} = \langle \mathring{r}_E^2 \rangle - \frac{23}{2}(4\pi f_\pi^2 R^4)\frac{m_\pi}{M_N} + \ldots, \qquad \text{(I6)}$$

which is, however, not yet the complete result for the following reason. The chiral expansion of the exact model expression for the energy density (43) in the gradient expansion contains—in addition to Eq. (52)—also the term

$$\rho_E(r)_{\text{part 2}} = \frac{m_\pi^2 f_\pi^2}{4}\,\text{tr}_F(2 - U - U^\dagger) = m_\pi^2 f_\pi^2(1 - \cos P(r)). \qquad \text{(I7)}$$

This term is of "zeroth order" in the gradient expansion. It arises from the current quark mass term in (25) and is related to the nucleon-pion sigma-term in the gradient expansion [33]. The explicit appearance of the current quark mass has been eliminated in (I7) in favor of m_π^2 by means of the Gell-Mann-Oakes-Renner relation which is valid in the model. The m_π^2 term (I7) vanishes in the chiral limit, and was therefore not displayed in (52), but it contributes in linear m_π order to (I6). This may not be obvious at a first glance; however, from (I7) we obtain

$$\langle r_E^2 \rangle_{\text{part 2}} = -4\pi f_\pi^2 R^4 \frac{m_\pi}{M_N}\int_0^\infty dz \times \frac{z^8(z^3 - 2z - 1)e^{-2z} - 4a^4 z^4(1+z)^4}{(z^4 + a^4(1+z)^2 e^{-4z})^2}\Bigg|_{a=0} + \ldots = \frac{5}{2}(4\pi f_\pi^2 R^4)\frac{m_\pi}{M_N} + \ldots, \qquad \text{(I8)}$$

and adding up (I6) and (I8) we obtain

$$\langle r_E^2 \rangle = \langle \mathring{r}_E^2 \rangle - 9(4\pi f_\pi^2 R^4)\frac{m_\pi}{M_N} + \ldots \qquad \text{(I9)}$$

It is not necessary to consider chiral corrections due to the nucleon mass $M_N = \mathring{M}_N + Bm_\pi^2 + \ldots$ because they contribute only at higher orders. (Notice that the CQSM also consistently describes the chiral expansion of M_N [33].) Eliminating $R = \sqrt{A/2}$ in (I9) by means of (29) yields finally the results for $\langle r_E^2 \rangle$ in (53) and for $M_2'(0)$ in (66).

Finally we comment on the form factor $J(t)$. Also in this case the normalization is trivial, since $J(0) = \frac{1}{2}$, but e.g. the chiral expansion of $J'(0) = \frac{1}{6}\langle r_J^2 \rangle$ is of interest. Here we restrict ourselves to the mere observation that $\langle r_J^2 \rangle$ diverges in the chiral limit.

In contrast to $M_2(t)$ and $d_1(t)$, which are nonzero in the leading order of the large-N_c expansion, $J(t)$ arises from $1/N_c$ (rotational) corrections. For such quantities the noncommutativity of the large-N_c and chiral limit may have more drastic implications [51]. For example, in the slowly rotating soliton approach (as realized e.g. in the Skyrme model in Ref. [93]) the isovector electric mean square radius diverges as $1/m_\pi$ in the chiral limit—in contrast to $\ln m_\pi$ at finite N_c. For $\langle r_J^2 \rangle$ the situation is completely analog—as a study in the Skyrme model reveals [94].

[1] H. R. Pagels, Phys. Rev. **144**, 1250 (1966).
[2] D. Müller, D. Robaschik, B. Geyer, F. M. Dittes, and J. Hořejši, Fortschr. Phys. **42**, 101 (1994).
[3] X. D. Ji, Phys. Rev. Lett. **78**, 610 (1997); Phys. Rev. D **55**, 7114 (1997).
[4] A. V. Radyushkin, Phys. Rev. D **56**, 5524 (1997).
[5] J. C. Collins, L. Frankfurt, and M. Strikman, Phys. Rev. D **56**, 2982 (1997).
[6] P. R. B. Saull (ZEUS Collaboration), arXiv:hep-ex/0003030.
[7] C. Adloff *et al.* (H1 Collaboration), Phys. Lett. B **517**, 47 (2001).

[8] A. Airapetian *et al.* (HERMES Collaboration), Phys. Rev. Lett. **87**, 182001 (2001).

[9] S. Stepanyan *et al.* (CLAS Collaboration), Phys. Rev. Lett. **87**, 182002 (2001).

[10] F. Ellinghaus (HERMES Collaboration), Nucl. Phys. **A711**, 171 (2002).

[11] S. Chekanov *et al.* (ZEUS Collaboration), Phys. Lett. B **573**, 46 (2003).

[12] A. Aktas *et al.* (H1 Collaboration), Eur. Phys. J. C **44**, 1 (2005).

[13] C. Muñoz Camacho *et al.* (Jefferson Lab Hall A Collaboration), Phys. Rev. Lett. **97**, 262002 (2006).

[14] A. Airapetian *et al.* (HERMES Collaboration), Phys. Rev. D **75**, 011103 (2007).

[15] X. D. Ji, J. Phys. G **24**, 1181 (1998).

[16] A. V. Radyushkin, in *At the Frontier of Particle Physics*, edited by M. Shifman (World Scientific, Singapore, 2001), vol. 1, pp. 1037–1099.

[17] K. Goeke, M. V. Polyakov, and M. Vanderhaeghen, Prog. Part. Nucl. Phys. **47**, 401 (2001).

[18] M. Diehl, Phys. Rep. **388**, 41 (2003).

[19] A. V. Belitsky, D. Mueller, and A. Kirchner, Nucl. Phys. **B629**, 323 (2002).

[20] A. V. Belitsky and A. V. Radyushkin, Phys. Rep. **418**, 1 (2005).

[21] M. V. Polyakov, Phys. Lett. B **555**, 57 (2003).

[22] M. V. Polyakov and A. G. Shuvaev, arXiv:hep-ph/0207153.

[23] R. G. Sachs, Phys. Rev. **126**, 2256 (1962).

[24] M. Burkardt, Phys. Rev. D **62**, 071503 (2000); **66**, 119903(E) (2002); Int. J. Mod. Phys. A **18**, 173 (2003).

[25] J. P. Ralston and B. Pire, Phys. Rev. D **66**, 111501 (2002).

[26] M. Diehl, Eur. Phys. J. C **25**, 223 (2002); **31**, 277(E) (2003).

[27] D. I. Diakonov and V. Y. Petrov, Pis'ma Zh. Eksp. Teor. Fiz. **43**, 57 (1986) [JETP Lett. **43**, 75 (1986)].

[28] D. I. Diakonov, V. Y. Petrov, and P. V. Pobylitsa, Nucl. Phys. **B306**, 809 (1988); D. I. Diakonov, V. Y. Petrov, and M. Praszałowicz, Nucl. Phys. **B323**, 53 (1989).

[29] E. Witten, Nucl. Phys. **B160**, 57 (1979); **B223**, 433 (1983).

[30] C. V. Christov, A. Z. Górski, K. Goeke, and P. V. Pobylitsa, Nucl. Phys. **A592**, 513 (1995).

[31] C. V. Christov *et al.*, Prog. Part. Nucl. Phys. **37**, 91 (1996).

[32] C. Schüren, E. Ruiz Arriola, and K. Goeke, Nucl. Phys. **A547**, 612 (1992).

[33] P. Schweitzer, Phys. Rev. D **69**, 034003 (2004).

[34] D. I. Diakonov, V. Y. Petrov, P. V. Pobylitsa, M. V. Polyakov, and C. Weiss, Nucl. Phys. **B480**, 341 (1996).

[35] D. I. Diakonov, V. Y. Petrov, P. V. Pobylitsa, M. V. Polyakov, and C. Weiss, Phys. Rev. D **56**, 4069 (1997); **58**, 038502 (1998); P. V. Pobylitsa and M. V. Polyakov, Phys. Lett. B **389**, 350 (1996).

[36] P. V. Pobylitsa, M. V. Polyakov, K. Goeke, T. Watabe, and C. Weiss, Phys. Rev. D **59**, 034024 (1999); C. Weiss and K. Goeke, arXiv:hep-ph/9712447.

[37] M. Wakamatsu and T. Kubota, Phys. Rev. D **60**, 034020 (1999).

[38] K. Goeke, P. V. Pobylitsa, M. V. Polyakov, P. Schweitzer, and D. Urbano, Acta Phys. Pol. B **32**, 1201 (2001).

[39] P. Schweitzer, D. Urbano, M. V. Polyakov, C. Weiss, P. V. Pobylitsa, and K. Goeke, Phys. Rev. D **64**, 034013 (2001).

[40] V. Y. Petrov, P. V. Pobylitsa, M. V. Polyakov, I. Börnig, K. Goeke, and C. Weiss, Phys. Rev. D **57**, 4325 (1998).

[41] M. Penttinen, M. V. Polyakov, and K. Goeke, Phys. Rev. D **62**, 014024 (2000).

[42] P. Schweitzer, S. Boffi, and M. Radici, Phys. Rev. D **66**, 114004 (2002).

[43] P. Schweitzer, M. Colli, and S. Boffi, Phys. Rev. D **67**, 114022 (2003); P. Schweitzer, S. Boffi, and M. Radici, Nucl. Phys. **A711**, 207 (2002).

[44] J. Ossmann, M. V. Polyakov, P. Schweitzer, D. Urbano, and K. Goeke, Phys. Rev. D **71**, 034011 (2005).

[45] M. Wakamatsu and H. Tsujimoto, Phys. Rev. D **71**, 074001 (2005).

[46] M. Wakamatsu and Y. Nakakoji, Phys. Rev. D **74**, 054006 (2006).

[47] J. W. Chen and X. D. Ji, Phys. Rev. Lett. **88**, 052003 (2002).

[48] A. V. Belitsky and X. Ji, Phys. Lett. B **538**, 289 (2002).

[49] M. Diehl, A. Manashov, and A. Schäfer, Eur. Phys. J. A **29**, 315 (2006).

[50] R. F. Dashen, E. Jenkins, and A. V. Manohar, Phys. Rev. D **49**, 4713 (1994); **51**, 2489(E) (1995).

[51] T. D. Cohen and W. Broniowski, Phys. Lett. B **292**, 5 (1992); T. D. Cohen, arXiv:hep-ph/9512275.

[52] N. Mathur, S. J. Dong, K. F. Liu, L. Mankiewicz, and N. C. Mukhopadhyay, Phys. Rev. D **62**, 114504 (2000).

[53] V. Gadiyak, X. D. Ji, and C. W. Jung, Phys. Rev. D **65**, 094510 (2002).

[54] P. Hägler, J. Negele, D. B. Renner, W. Schroers, T. Lippert, and K. Schilling (LHPC Collaboration), Phys. Rev. D **68**, 034505 (2003).

[55] M. Göckeler, R. Horsley, D. Pleiter, P. E. L. Rakow, A. Schäfer, G. Schierholz, and W. Schroers (QCDSF Collaboration), Phys. Rev. Lett. **92**, 042002 (2004).

[56] J. W. Negele *et al.*, Nucl. Phys. B, Proc. Suppl. **128**, 170 (2004).

[57] W. Schroers, arXiv:hep-lat/0701003; Nucl. Phys. B, Proc. Suppl. **153**, 277 (2006).

[58] K. Goeke, J. Ossmann, P. Schweitzer, and A. Silva, Eur. Phys. J. A **27**, 77 (2006).

[59] K. Goeke, J. Grabis, J. Ossmann, P. Schweitzer, A. Silva, and D. Urbano, arXiv:hep-ph/0702031 [Phys. Rev. C. (to be published)].

[60] J. F. Donoghue and H. Leutwyler, Z. Phys. C **52**, 343 (1991).

[61] B. Kubis and U. G. Meissner, Nucl. Phys. **A671**, 332 (2000); **A692**, 647(E) (2001).

[62] E. Megias, E. Ruiz Arriola, L. L. Salcedo, and W. Broniowski, Phys. Rev. D **70**, 034031 (2004); E. Megias, E. Ruiz Arriola, and L. L. Salcedo, Phys. Rev. D **72**, 014001 (2005).

[63] D. Brommel *et al.*, Proc. Sci., LAT2005 (2006) 360.

[64] J. W. Chen, W. Detmold, and B. Smigielski, Phys. Rev. D **75**, 074003 (2007).

[65] F. Ellinghaus, W. D. Nowak, A. V. Vinnikov, and Z. Ye, Eur. Phys. J. C **46**, 729 (2006).

[66] M. V. Polyakov and C. Weiss, Phys. Rev. D **60**, 114017 (1999).

[67] O. V. Teryaev, Phys. Lett. B **510**, 125 (2001).

[68] N. Kivel, M. V. Polyakov, and M. Vanderhaeghen, Phys. Rev. D **63**, 114014 (2001).

[69] V. Guzey and M. Siddikov, J. Phys. G **32**, 251 (2006).
[70] S. L. Adler, J. C. Collins, and A. Duncan, Phys. Rev. D **15**, 1712 (1977).
[71] N. K. Nielsen, Nucl. Phys. **B120**, 212 (1977).
[72] J. C. Collins, A. Duncan, and S. D. Joglekar, Phys. Rev. D **16**, 438 (1977).
[73] For a recent review see: S. L. Adler, arXiv:hep-th/0405040.
[74] D. I. Diakonov and V. Y. Petrov, Nucl. Phys. **B245**, 259 (1984).
[75] D. I. Diakonov and V. Y. Petrov, Nucl. Phys. **B272**, 457 (1986).
[76] D. Diakonov, M. V. Polyakov, and C. Weiss, Nucl. Phys. **B461**, 539 (1996).
[77] For reviews see, D. I. Diakonov and V. Y. Petrov, in *At the Frontier of Particle Physics*, edited by M. Shifman (World Scientific, Singapore, 2001), vol. 1, pp. 359–415; D. Diakonov, Prog. Part. Nucl. Phys. **51**, 173 (2003); arXiv:hep-ph/0406043.
[78] D. I. Diakonov and M. I. Eides, Pis'ma Zh. Eksp. Teor. Fiz. **38**, 358 (1983) [JETP Lett. **38**, 433 (1983)].
[79] A. Dhar, R. Shankar, and S. R. Wadia, Phys. Rev. D **31**, 3256 (1985).
[80] S. Kahana and G. Ripka, Nucl. Phys. **A429**, 462 (1984).
[81] T. Kubota, M. Wakamatsu, and T. Watabe, Phys. Rev. D **60**, 014016 (1999).
[82] P. V. Pobylitsa, E. Ruiz Arriola, T. Meissner, F. Grummer, K. Goeke, and W. Broniowski, J. Phys. G **18**, 1455 (1992).
[83] M. Prakash, J. M. Lattimer, J. A. Pons, A. W. Steiner, and S. Reddy, Lect. Notes Phys. **578**, 364 (2001).
[84] M. Diehl, T. Feldmann, R. Jakob, and P. Kroll, Eur. Phys. J. C **39**, 1 (2005).
[85] M. Guidal, M. V. Polyakov, A. V. Radyushkin, and M. Vanderhaeghen, Phys. Rev. D **72**, 054013 (2005).
[86] A. Radyushkin, Ann. Phys. (N.Y.) **13**, 718 (2004).
[87] M. Vanderhaeghen, Ann. Phys. (N.Y.) **13**, 740 (2004).
[88] V. M. Braun, P. Górnicki, L. Mankiewicz, and A. Schäfer, Phys. Lett. B **302**, 291 (1993).
[89] O. V. Teryaev, arXiv:hep-ph/9803403; arXiv:hep-ph/9904376.
[90] M. Diehl, T. Gousset, B. Pire, and O. Teryaev, Phys. Rev. Lett. **81**, 1782 (1998).
[91] A. Freund, A. V. Radyushkin, A. Schäfer, and C. Weiss, Phys. Rev. Lett. **90**, 092001 (2003).
[92] J. D. Bjorken and S. D. Drell, *Relativistic Quantum Fields* (Mc Graw-Hill, New York, 1965).
[93] G. S. Adkins and C. R. Nappi, Nucl. Phys. **B233**, 109 (1984).
[94] C. Cebulla, K. Goeke, J. Ossmann, M. V. Polyakov, and P. Schweitzer arXiv:hep-ph/0703025.
[95] M. Wakamatsu, Phys. Lett. B **648**, 181 (2007).